A putative loop connection between VTA dopamine neurons and nucleus accumbens encodes positive valence to compensate for hunger

Xiao Cui [1], Qiuping Tong [1], Hao Xu, Chuantong Xie, Lei Xiao [*]

Department of Orthodontics, Shanghai Stomatological Hospital & School of Stomatology, The State Key Laboratory of Medical Neurobiology, MOE Frontiers Center for Brain Science, and the Institutes of Brain Science, Fudan University, Shanghai 200032, China

ARTICLE INFO

ABSTRACT

Dopamine (DA) signal play pivotal roles in regulating motivated behaviors, including feeding behavior, but the role of midbrain DA neurons in modulating food intake and neural circuitry mechanisms remain largely unknown. Here, we found that activating but not inhibiting ventral tegmental area (VTA) DA neurons reduces mouse food intake. Furthermore, DA neurons in ventral VTA, especially neurons projecting to the medial nucleus accumbens (NAc), are activated by refeeding in the 24 h fasted mice. Combing neural circuitry tracing, optogenetic, chemogenetic, and pharmacological manipulations, we established that the VTA→medial NAc→VTA loop circuit is critical for the VTA DA neurons activation-induced food intake reduction. Moreover, activating either VTA DA neurons or dopaminergic axons in medial NAc elevates positive valence, which will compensate for the hungry-induced food intake. Thus, our study identifies a subset of positive valence-encoded VTA DA neurons forming possible loop connections with medial NAc that are anorexigenic.

1. Introduction

Obesity is becoming one of the major risk factors for death globally (GBD, Risk Factor Collaborators, 2017, 2018). During the COVID-19 pandemic, obesity is found to be associated with worse outcomes in patients (Hajifathalian et al., 2020; Popkin et al., 2020). Dis-balancing between food intake and energy expenditure is the main reason to cause excessive energy and obesity (Heymsfield and Wadden, 2017). Overconsumption of food is considered to be a significant risk factor of the obesity epidemic (Swinburn et al., 2011). Several hypothalamic nuclei, such as arcuate nucleus (ARC), ventral medial hypothalamus (VMH), dorsal medial hypothalamus (DMN), paraventricular nucleus of the hypothalamus (PVH), and lateral hypothalamus (LH), are suggested to form appetite regulation network to maintain body energy homeostasis (Alcantara et al., 2022; Morton et al., 2006; Roh et al., 2016). In addition to these hypothalamic regions, the limbic reward system is also involved in regulating food intake (Morton et al., 2006; Rossi and Stuber, 2018). However, the limbic reward neurocircuitry underlying feeding regulation has not been fully understood.

Dopamine (DA) is the main neurotransmitter/neuromodulator associated with motivation, reward, and pleasure. The mesolimbic DA system, originating from DA neurons in the ventral tegmental area (VTA), is activated in response to palatable food and is involved in modulating food consumption (Kenny, 2011), and this system is presumed to be the core in mediating hedonic feeding. However, DA-deficient mice stopped feeding and died a few weeks after birth, and these mice could be rescued to restore homeostatic feeding by administrating 3,4- dihydroxy-L-phenylalanine (L-DOPA) or restoring DA production within the caudate putamen (Szczypka et al., 2001, 1999; Zhou and Palmiter, 1995), which indicates that DA signal is also important for homeostatic feeding. The role of VTA DA neurons in regulating feeding behaviors remains controversial. Some metabolic signals, including leptin, insulin, and ghrelin, are reported to promote/reduce food intake by directly exciting/inhibiting VTA DA neuronal activity (Abizaid et al., 2006; Hommel et al., 2006; Mebel et al., 2012). Endogenous glucagon-like peptide-1 (GLP-1) reduces food intake by suppressing the excitatory synaptic inputs to VTA DA neurons (Wang et al., 2015). These studies suggested a positive relationship between VTA DA neuronal activity and food intake. However, chemogenetic or optogenetic activation of VTA DA neurons tended to decrease feeding behavior at food-restricted state or have no significant effect on food intake in sated animals (Boekhoudt et al., 2017; Marino et al., 2020), but a study reported the opposite effect during pellet retrieval consumption (Mazzone et al., 2020). A recent study showed that cerebellar output increased striatal

* Corresponding author.
  E-mail address: leixiao@fudan.edu.cn (L. Xiao).
[1] X.C. and Q.T. contributed equally to this work.

DA from VTA DA neurons to reduce food intake (Low et al., 2021). Hence, the effects of VTA DA signal on feeding regulation are complex and needed to be further explored.

The diversity of VTA DA neurons in gene expressions, cellular properties, and neural circuits contributes to the distinct and even opposite functions (Beier et al., 2019, 2015; Engelhard et al., 2019; Lammel et al., 2012, 2008; Poulin et al., 2018; Saunders et al., 2018). Though VTA DA neurons are reported to be involved in regulating feeding behavior, whether a specific subtype of VTA DA neurons or dopaminergic neural circuit is responsible for this behavior is still not clear. Recent studies suggested that parabrachial nucleus (PBN) and dorsal raphe nucleus (DRN) are two identified targets of VTA DA neurons involved in regulating food intake (Cai et al., 2022; Han et al., 2021). Nucleus accumbens (NAc) is one of the primary targets of VTA DA neurons and plays a pivotal role in feeding and reward behaviors (Gendelis et al., 2021). DA release in NAc controls reward-seeking behaviors (Klawonn and Malenka, 2018; Wise and Robble, 2020), and NAc DA level is negatively correlated with food intake (Low et al., 2021). However, restoration of DA production in the NAc was reported to restore preference for sucrose or a palatable diet, but did not rescue the homeostatic feeding behavior in the DA-deficient mice (Szczypka et al., 2001), and activating VTA DA axons in NAc was reported to have a weak effect on food intake (Boekhoudt et al., 2017; Han et al., 2021). NAc is composed of several subnuclei, which have distinct neural connections with VTA subregions and DA neurons to play different functions (de Jong et al., 2019; Yang et al., 2018). Neural circuits of VTA DA neurons underlying feeding regulation, especially connection with NAc subregions, should be further dissected.

In the present study, we investigated the role of VTA DA neurons in regulating feeding behavior and identified the possible neural circuitry mechanism by combining chemogenetic, optogenetic, neural circuitry tracing, pharmacological, and behavioral methods. In addition, we assessed the compensatory effect between positive valence encoded by VTA DA neurons/neural circuit and food intake in the hungry state.

2. Results

2.1. Activating VTA DA neurons reduces food intake, but silencing DA neurons has a weak effect

Since the role of VTA DA neurons in regulating feeding behavior remains unclear, we first used both chemogenetic and optogenetic methods to directly manipulate the activity of VTA DA neurons with DAT-Cre transgenic mice and measured the food intake in different conditions (Fig. 1A-1F). Chemogenetical activating VTA DA neurons with hM3Dq-mCherry expression by intraperitoneal (i.p.) injection of clozapine N-oxide (CNO) significantly reduced the food intake in normal feeding mice, 24 h fasted mice, and 36 h fasted mice (Fig. S1A; Fig. 1C). In the presence of the high-fat (HF) food, activating VTA DA neurons also significantly decreased the food intake in the 24 h fasted mice (Fig. 1C). Surprisingly, chemogenetical inhibition of VTA DA neurons expressing hM4Di-mCherry viruses did not significantly change the food intake (Fig. S1B; Fig. 1D). CNO application did not affect food intake in mice with only mCherry expression in VTA DA neurons (Figure S1C).

We further expressed ChR2-mCherry viruses into VTA DA neurons and observed that activating VTA DA neurons with 10-ms 20 Hz, but not 5 Hz or 10 Hz, light stimulation tended to reduce the food intake in the 24 h fasted mice (Fig. 1E-1 G and Figure S1D). For the mice with only mCherry expression in VTA DA neurons, 20 Hz light stimulation did not change the food intake in the 24 h fasted mice (Fig. 1G). Activating VTA DA neurons with 20 Hz light stimulation significantly reduced the time spent at the food zone and the feeding time in the 24 h fasted mice (Fig. 1H; Fig. S1E). Similar to the chemogenetic inhibition, optogenetic silencing VTA DA neurons with eNpHR3.0-eYFP expression had no significant effect on mouse food intake and time spent in the

food zone (Figure S1F-S1G). No significant gender differences were observed in the effects of manipulating VTA DA neurons on food intake (Figure S2).

We also investigated the effects of long-term activating/inhibiting VTA DA neurons on mouse body weight and food intake. AAV-DIO-hM3Dq/hM4Di-mCherry viruses were injected into the VTA of DAT-Cre mice. 4 weeks after virus injection, mice were separately housed with intraperitoneal (i.p.) injection of saline (SAL) for 7 consecutive days, and mice were then randomly divided into control group (SAL injection) and experiment group (CNO injection) (Fig. 1I). Mouse body weight and food intake were monitored every day, and we observed that chronic chemogenetic approach for activating VTA DA neurons significantly decreased mouse body weight and the food intake relative to body weight (Fig. 1J, Figure S1H-S1I), but silencing VTA DA neurons had no significant effects (Fig. 1K, Figure S1J-S1K). Together, all of these results suggest an anorexigenic role of VTA DA neurons.

2.2. Medial NAc-projecting ventral VTA DA neurons are activated after refeeding and reduce food intake in the fasted mice

VTA DA neurons are diverse in functions according to their spatial distributions and diverse neural circuits (Beier et al., 2019, 2015; Engelhard et al., 2019; Lammel et al., 2012, 2008). We then investigated the activity change of VTA DA neurons after 2 h refeeding in 24 h fasted mice. The cFos expression in VTA has been detected in the fasting and refeeding conditions (Fig. 2A and Fig. S3A), and the total number of cFos positive neurons in VTA was similar in these two conditions (Figure S3B), but the ratio of the TH and cFos double-positive neurons was significantly increased in both male and female mice in the refeeding condition compared to the fasting condition (Fig. 2A-2B; Figure S3C). The number of the TH and cFos double-positive neurons also tended to increase in the refeeding condition (Figure S3B). Meanwhile, we observed that the cFos and TH double-positive neurons in the refeeding condition were mainly distributed in the medial and ventral VTA subregions, i.e. the paranigral nucleus (PN) and interfascicular nucleus (IF) (Fig. 2C-2D and Figure S3A). Since VTA contained a similar number of cFos-positive neurons in the fasting and refeeding conditions, we detected the cFos expression in VTA GABA neurons in fasting and refeeding conditions. With the GAD-Cre; Ai3 transgenic mice to label GABA neurons, we observed that more VTA GABA neurons were cFos positive in the fasting condition, and the proportion of GABA and cFos double-positive neurons was reduced in the refeeding condition (Fig. 2E; Fig. S3D-S3E). These results indicated the opposite role of VTA DA neurons and GABA neurons in regulating food intake. Contrary to activating VTA DA neurons, optogenetic activating VTA GABA neurons significantly increased mouse food intake and the time spent in the food zone after 24 h fasting, and activating VTA glutamatergic neurons had no significant effect (Figure S3F-S3H). Therefore, DA neurons in ventral VTA may be involved in reducing food intake in fasted mice.

VTA DA neurons project to a lot of brain regions, including the medial prefrontal cortex (mPFC), nucleus accumbens (NAc), lateral septum (LS), lateral hypothalamus (LH), amygdala (Amy), ventral hippocampus (vHipp), and parabrachial nucleus (PBN), and some of the downstream regions are reported to regulate feeding behavior (Z. Chen et al., 2022; Land et al., 2014; O'Connor et al., 2015; Shivacharan et al., 2022; Stuber and Wise, 2016). Combining retrograde tracing and cFos immunolabeling, we investigated possible target(s) of the ventral VTA DA neurons in regulating food intake. Fluoro-Gold (FG) is a retrograde tracer and widely used to label the neurons projecting to the FG injection region. We separately injected FG into the mPFC, medial NAc, lateral NAc, LS, LH, Amy, vHipp, and PBN regions of wildtype (WT) mice (Figure S4A), and the refeeding-induced cFos expression in VTA was detected in the 24 h fasted mice (Fig. 2F-2 G). Around 50% of VTA TH, cFos double-
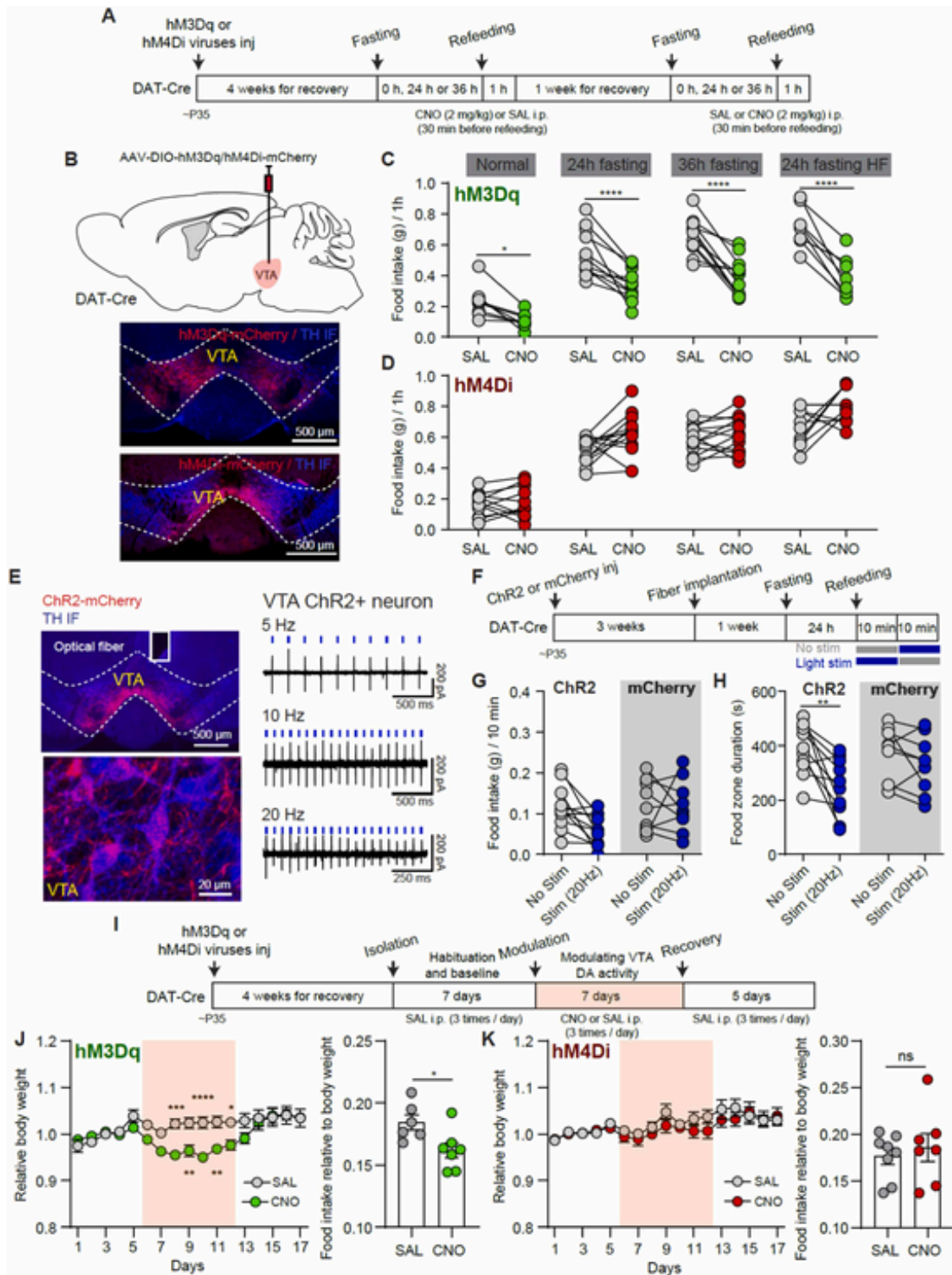
Fig. 1. Activation of VTA DA neurons reduces mouse food intake, but inhibiting VTA DA neurons has a weak effect. (A) Experimental procedure for investigating the effect of acutely modulating VTA DA neuronal activity on food intake with chemogenetic method. (B) Schematic of viral delivering (Top) and examples of hM3Dq-mcherry and hM4Di-mcherry virus expression in the VTA DA neurons, labeled by tyrosine hydroxylase (TH) immunostaining (Bottom). (C) Summary about effects of chemogenetic activating VTA DA neurons on food intake in normal feeding mice, 24 h fasted mice, 36 h fasted mice, and 24 h fasted mice with high-fat (HF) food intake. $n = 8$ mice for normal feeding, 11 mice for 24 h fasting condition, 11 mice for 36 h fasting condition, and 8 mice for 24 h fasting with HF food intake condition. RM two-way ANOVA, main effect of CNO, $F_{(1, 34)} = 110.9$, $p < 0.001$; fasting state, $F_{(3, 34)} = 25.78$, $p < 0.0001$ and interaction, $F_{(3, 34)} = 3.599$, $p = 0.0232$. Sidak's multiple comparison test, $* p < 0.05$, $**** p < 0.0001$. (D) Same as (C), but for chemogenetic inhibiting VTA DA neurons. $n = 11$ mice for normal feeding, 13 mice for 24 h fasting condition, 13 mice for 36 h fasting condition, and 9 mice for 24 h fasting with HF food intake condition. RM two-way ANOVA, main effect of CNO, $F_{(1, 42)} = 13.87$, $p = 0.0006$; fasting state, $F_{(3, 42)} = 86.89$, $p < 0.0001$ and interaction, $F_{(3, 42)} = 2.042$, $p = 0.1225$. (E)

Fig. 1.—*continued*

Example images showing ChR2-mCherry expression in VTA DA neurons and optical fiber implantation in VTA (Left) and the example of blue light stimulation-induced firing activity (Right). (F) Experimental procedure for the optogenetic experiment. (G) Summary about light stimulation in VTA on food intake for mice with ChR2-mCherry and only mCherry expression in VTA DA neurons. $n = 11$ mice for ChR2-mCherry expression and 9 mice for mCherry expression. RM two-way ANOVA, main effect of light stimulation, $F(1, 18) = 2.743$, $p = 0.1150$; virus expression, $F(1, 18) = 3.306$, $p = 0.0857$ and interaction, $F(1, 18) = 3.277$, $p = 0.0870$. While the pattern of results in ChR2 group fit within the hypothesis, the study was not sufficiently powered to detect a significant interaction. (H) Summary about light stimulation in VTA on the time spent in food zone for mice with ChR2-mCherry and only mCherry expression in VTA DA neurons. RM two-way ANOVA, main effect of light stimulation, $F(1, 18) = 006875$, $p = 0.4179$; virus expression, $F(1, 18) = 13.19$, $p = 0.0019$ and interaction, $F(1, 18) = 5.163$, $p = 0.0356$. Sidak's multiple comparison test, $* * p < 0.01$. (I) Experimental procedure for long-term chemogenetic activation/inhibition of VTA DA neurons. (J) Left: Effect of long-term chemogenetic activation of VTA DA neurons on the relative body weight change. The pink shadow indicates saline (SAL) or clozapine N-oxide (CNO) injection these days. RM two-way ANOVA, main effect of day, $F(16, 185) = 6.319$, $p < 0.0001$; CNO, $F(1, 185) = 40.61$, $p < 0.0001$ and interaction, $F(16, 185) = 3.516$, $p < 0.0001$. Sidak's multiple comparison test, $* p < 0.05$, $* * p < 0.01$, $* * * p < 0.001$, $* * * * p < 0.0001$. Right: Summary about the food intake relative to body weight when activation of VTA DA neurons. $n = 6$ mice for hM3Dq-SAL and 7 mice for hM3Dq-CNO, $* p < 0.05$, unpaired *t*-test. (K) Same as (J), but for long-term chemogenetic inhibition of VTA DA neurons. $n = 8$ mice for hM4Di-SAL and 7 mice for hM4Di-CNO. RM two-way ANOVA, main effect of day, $F(16, 221) = 3.861$, $p < 0.0001$; CNO, $F(1, 221) = 4.814$, $p = 0.0293$ and interaction, $F(16, 221) = 0.5443$, $p = 0.9211$.

positive neurons were co-localized with the FG signal when FG was injected into the medial NAc region (Fig. 2G-2 H). We also observed some VTA TH, cFos double-positive neurons were labeled by FG signal when the FG was injected into the lateral NAc, LS, Amy, and LH, but no overlap was detected when the FG was injected into mPFC, vHipp, or PBN (Fig. 2G-2 H, Figure S4B).

NAc, LH, and LS are reported to regulate food intake (Z. Chen et al., 2022; Gendelis et al., 2021; Stuber and Wise, 2016), so they are the candidate target regions of VTA DA neurons to modulate feeding behavior. We then investigated whether the projections of VTA DA to these possible regions are involved in regulating food intake. Firstly, with DAT-Cre mice, we specifically activated the VTA DA neurons projecting to these three regions separately with RetroAAV-Flex-Flpo viruses injected into the target regions and AAV-fDIO-ChR2-eYFP viruses injected into the VTA with optical fiber implanted in VTA (Fig. 2I). Only the Cre-positive neurons projecting to the RetroAAV-Flex-Flpo viruses injected region will express Flp recombinase, which will further induce the expression of Flpo-dependent AAV-fDIO-ChR2-eYFP viruses in neurons. eYFP labeled neurons with RetroAAV-Flex-Flpo injected into the medial NAc were found to overlap with TH and cFos signal in ventral VTA after refeeding in 24 h fasted mice (Fig. 2I). Activating VTA DA neurons projecting to the medial NAc, but not LH or LS, tended to reduce mouse food intake in the 24 h fasted mice (Fig. 2J). The time spent at the food zone did not significantly change when activating VTA DA neurons projecting to these regions (Figure S4C). To further validate, we directly activated dopaminergic axons to induce the local DA release in these downstream regions with optogenetic method (Fig. 2K). Bilaterally activating VTA dopaminergic axons in medial NAc significantly reduced 24 h fasted mouse food intake and the time spent at the food zone, and no significant change was observed in the mice with only mCherry virus expression (Fig. 2L) or when activating dopaminergic axons in LH or LS (Figure S4D-S4E). Hence, our study provides conclusive evidence for medial NAc may be the main target of ventral VTA DA neurons to reduce food intake.

We further investigated the necessity of VTA dopaminergic projection to medial NAc in reducing food intake by combining optogenetic and pharmacological methods (Fig. 2M). High-frequency stimulation-induced DA release will mainly activate DA Drd1 receptors to increase neuronal activity (Cai et al., 2022). We found that VTA DA activation-induced food intake and food zone duration reductions disappeared after blocking DA Drd1 receptors with SCH23390 application in the medial NAc (Fig. 2N). Taken together, activating the VTA-medial NAc dopaminergic circuit reduces mouse food intake.

2.3. Ventral VTA DA neurons form a possible positive loop with medial NAc in regulating food intake

Since medial NAc is the main target of ventral VTA DA neurons to reduce mouse food intake in the hungry state (Fig. 2), and stimulating VTA-projecting NAc D1 neurons was also reported to inhibit food consumption (Bond et al., 2020), we inferred that ventral VTA DA neurons may form loop connection with medial NAc neurons to reduce mouse food intake. scAAV1-hSyn-Cre viruses have the anterograde transsynaptic property (Zingg et al., 2020), so we injected scAAV1-hSyn-Cre into the VTA and Cre-dependent AAV-DIO-eYFP into medial NAc to label the postsynaptic neurons of VTA in the medial NAc. We also injected FG into the VTA to label the neurons projecting to the VTA and checked the overlap between eYFP signal and FG in the medial NAc. With both retrograde and anterograde tracing methods, we observed that some medial NAc neurons received synaptic inputs from VTA and also projected to the VTA (Fig. 3A-3B). Summary results showed that ~50% of VTA-projecting NAc neurons received synaptic inputs from VTA (54.97% ± 9.34%, $n = 3$ mice), and ~15% NAc neurons receiving synaptic input from VTA project to the VTA (17.61% ± 3.49%, $n = 3$ mice) (Figure S5A). With similar retrograde and anterograde tracing methods, we found some VTA neurons receiving synaptic inputs from medial NAc also projected back to the NAc (Fig. 3C-3D), and about 50% of these neurons were TH positive (54.99% ± 6.36%, $n = 3$ mice) (Figure S5B). In addition to VTA DA neurons, ~50% of medial NAc-projecting VTA neurons were non-DA neurons (48.63% ± 1.27%, $n = 3$ mice) (Figure S5C).

Previous studies found that VTA-projecting NAc neurons are D1-positive GABAergic neurons and activating NAc neurons will excite some VTA DA neurons via disinhibiting VTA GABA neurons (Edwards et al., 2017; Liu et al., 2022). We further confirmed the effect of activating medial NAc neurons on the activity of VTA DA neurons, and observed that chemogenetic activation of medial NAc neurons significantly increased the cFos expression in VTA and VTA DA neurons (Fig. 3E-3 F and Figure S5D). Specifically activating medial NAc D1 neurons also significantly increased the cFos expression in VTA DA neurons (Figure S5E). We also observed that more NAc-projecting ventral VTA DA neurons were cFos positive when activating NAc D1 neurons (Fig. 3G-3 H). With the current-clamp recording in slices of TH-GFP mice (Figure S5G), we found that the firing activity of ~30% ventral VTA GFP-positive (DA) neurons (5/16 DA neurons from 4 mice) was increased when expressing ChR2 viruses into medial NAc neurons and optogenetically activating the axons from medial NAc neurons (Fig. 3I-3 K). We also observed that ~50% VTA GFP-negative (non-DA) neurons (5/9 non-DA neurons from 4 mice) were inhibited when activating medial NAc neuronal axons (Figure S5F). Together, these results support that activating NAc D1 neurons is able to disinhibit some VTA DA neurons, especially the VTA DA neurons projecting to the medial NAc.

We further investigated the role of activating the VTA→medial NAc→VTA dopaminergic loop circuit on mouse feeding behavior. Be-
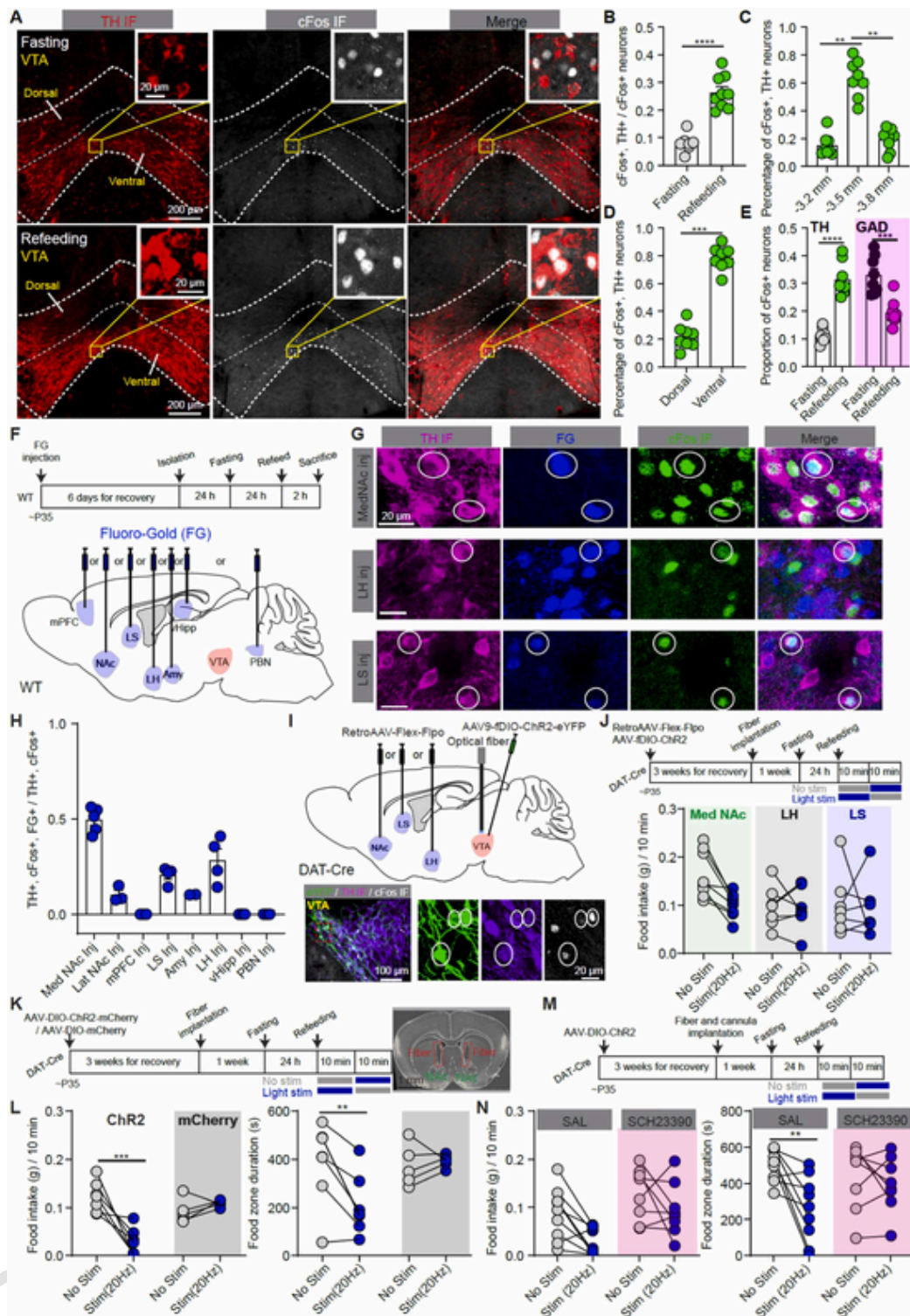
Fig. 2. Medial NAc-projecting ventral VTA DA neurons are activated after refeeding and reduce food intake in the fasted mice. (A) Images showing the colocalization between cFos neurons and VTA DA neurons, labeled by tyrosine hydroxylase (TH) immunostaining in the mice with 24 h fasting (Top) and 2 h refeeding after 24 h fasting (Bottom). Insets show enlarged views of the rectangle regions. (B) The ratio between TH, cFos double-positive neurons and total cFos positive neurons in fasting and refeeding conditions. $* ** * p < 0.0001$, unpaired t-test, $n = 7$ and 9 mice for the fasting and refeeding conditions, respectively. (C) The percentage distribution of cFos, TH double-positive neurons along VTA rostral-caudal axis in the refeeding mice. $n = 8$ mice, $* * p < 0.01$, one-way ANOVA with Tukey's post hoc test. (D) Same as (C), but for the distribution in dorsal and ventral VTA. (E) The overlap between cFos with VTA DA neurons (TH) and GABA neurons (GAD) in the fasting and refeeding conditions. RM two-way ANOVA, main effect of neuronal type, $F_{(1, 14)} = 3.552$, $p = 0.0804$; fasting state, $F_{(1, 14)} = 7.443$, $p = 0.0163$ and interaction, $F_{(1, 14)} = 84.28$, $p < 0.0001$. Sidak's multiple comparison test, $* ** p < 0.001$, $* ** * p < 0.0001$. $n = 8$ Gad-Cre; Ai3 mice for the fasting and refeeding conditions, respectively. (F) Experimental procedure for tracing the possible target(s) of VTA DA neurons with the Fluoro-Gold (FG) in wild-type (WT) mice. (G) Images showing the co-localization between TH, FG, and cFos signals in the VTA with FG injected into the medial NAc (Top), LH (Middle), and LS (Bot-

Fig. 2.—*continued*

tom), respectively. White circles indicate the TH, FG, and cFos triple positive neurons. (H) Summary about the percentage of VTA TH, cFos double-positive neurons co-localized with FG signal when FG was injected into the medial NAc, lateral NAc, mPFC, LS, LH, amygdala, vHipp, and PBN, respectively. (I) Top: The strategy used to manipulate VTA DA neurons projecting to medial NAc, LS, and LH. Bottom Left: An example image showing the overlap between fDIO-ChR2-eYFP, TH, and cFos signal in VTA with retroAAV-Flex-Flpo injected into the medial NAc. Bottom Right: The enlarged images with a red rectangle labeled on the Left. (J) Top: Experimental procedure. Bottom: Summary results about the food intake when activating VTA DA neurons projecting to the medial NAc, LH, and LS, respectively. RM two-way ANOVA, main effect of region, $F(2, 19) = 2.500$, $p = 0.1087$; light stimulation, $F(1, 19) = 3.904$, $p = 0.0629$ and interaction, $F(2, 19) = 2.050$, $p = 0.1563$. While the pattern of results in the medial NAc group fit within the hypothesis, the study was not sufficiently powered to detect a significant interaction. $n = 8, 7$, and 7 mice for medial NAc, LH, and LS. (K) Experimental procedure for activating VTA dopaminergic axons in medial NAc (Left) and the example with optical fibers bilaterally implanted into medial NAc (Right). (L) Summary about food intake (Left) and time spent at food zone (Right) when stimulating dopaminergic axons in the medial NAc with ChR2-mCherry or mCherry viruses expression in VTA DA neurons. For food intake, RM two-way ANOVA, main effect of light stimulation, $F(1, 10) = 9.154$, $p = 0.0128$; virus expression, $F(1, 10) = 9.139$, $p = 0.0128$ and interaction, $F(1, 10) = 18.87$, $p = 0.0015$. For food zone time, RM two-way ANOVA, main effect of light stimulation, $F(1, 10) = 6.512$, $p = 0.0288$; virus expression, $F(1, 10) = 1.767$, $p = 0.2133$ and interaction, $F(1, 10) = 9.972$, $p = 0.0102$. Sidak's multiple comparison test, $**p < 0.01$, $***p < 0.001$. $n = 7$ and 5 mice for ChR2 and mCherry, respectively. (M) Experimental procedure to pharmacologically block DA Drd1 receptors with local cannula infusion when optically activating VTA DA neurons. (N) Summary about food intake (Left) and time spent at food zone (Right) when activating VTA DA neurons and blocking medial NAc Drd1 receptors with SCH23390. For food intake, RM two-way ANOVA, main effect of light stimulation, $F(1, 15) = 8.784$, $p = 0.0097$; drug, $F(1, 15) = 8.526$, $p = 0.0128$ and interaction, $F(1, 15) = 0.6774$, $p = 0.4234$. While the pattern of results in the SAL group fit within the hypothesis, the study was not sufficiently powered to detect a significant interaction. For food zone time, RM two-way ANOVA, main effect of light stimulation, $F(1, 15) = 9.849$, $p = 0.0068$; drug, $F(1, 15) = 0.03581$, $p = 0.5585$ and interaction, $F(1, 15) = 4.965$, $p = 0.0416$. Sidak's multiple comparison test, $*p < 0.05$, $**p < 0.01$, $n = 9$ and 8 mice for SAL and SCH23390 groups.

cause of the technical limitations for us to specifically manipulate VTA DA neurons→medial NAc→VTA loop circuit, we firstly studied the role of VTA→medial NAc→VTA loop circuit in regulating feeding behavior. Combing anterograde transsynaptic tracing and optogenetic strategies, we injected scAAV1-hSyn-Cre into the VTA and AAV-DIO-ChR2-mCherry into the medial NAc of WT mice to express ChR2 into the VTA-projected NAc neurons, and implanted the optical fiber into the VTA to activate the axons from medial NAc neurons (Fig. 3L and Figure S5H). ChR2-mCherry were expressed in the soma of medial NAc neurons, and mCherry-positive axons, but not soma, were observed in the VTA (Figure S5H). We found that activating the VTA→medial NAc→VTA circuit significantly reduced food intake, tended to decrease the duration spent at the food zone (Fig. 3M), and also significantly reduced feeding time in the 24 h fasted mice (Figure S5I). Both VTA DA neurons and GABA neurons can send axons to the NAc, but in our study activation of VTA GABA neurons increased food intake (Figure S3G), which is opposite to the role of activating the VTA→medial NAc→VTA loop circuit, so we infer that VTA DA neurons projecting to medial NAc may be mainly involved in this loop circuit to regulate feeding behavior. The necessity of the medial NAc→VTA circuit in activating VTA DA neurons-induced food intake reduction was investigated. With DAT-Cre mice, Cre-dependent ChR2-EGFP was expressed in the VTA DA neurons and optical fiber was bilaterally implanted into the medial NAc. Meanwhile, hM4Di-mCherry was specific expressed into the VTA-projecting NAc neurons with RetroAAV-hSyn-Flpo and AAV-fDIO-hM4Di-mCherry injected into VTA and medial NAc, respectively (Fig. 3N). After inhibiting the VTA-projecting NAc neurons with the chemogenetic method, optically activating VTA dopaminergic axons in NAc had no significant effect on food intake or the duration spent at the food zone in the 24 h fasted mice (Figs. 3O and 3P). Taken together, VTA DA neurons form a possible positive loop with medial NAc to regulate mouse food intake.

2.4. Positive valence induced by activating the VTA→medial NAc→VTA loop circuit compensates for the hunger-induced food intake

Since neurons involved in satiation and hunger also encode positive and negative valence (He et al., 2021), we infer that activating VTA DA neurons or dopaminergic projection in medial NAc may induce positive valence, which will override the feeling of hunger in fasted mice. We combined optogenetic stimulation and the real-time place preference behavioral test to prove this hypothesis (Fig. 4A).

Firstly, optogenetic activation of VTA DA neurons in both normal feeding mice and 24 h fasted mice significantly increased the time spent on the light stimulation-paired side, and light stimulation did not affect the place preference in the mice with only mCherry expression (Fig. 4B-

4 C, Figure S6A and S6B). Secondly, when the optical fiber was bilaterally implanted into the medial NAc to activate VTA dopaminergic axons, light stimulation also tended to increase mouse preference for the light stimulation-paired side in both normal feeding and 24 h fasting conditions (Fig. 4D-4E, Figure S6A and S6B). Therefore, VTA DA neurons and their projection to medial NAc encode the positive valence property. Then, we examined whether the positive valence induced by activating VTA DA neurons and their projection to medial NAc is sufficient to override the hungry-induced feeding in the fasted mice. The 24 h fasted mice were placed in a three-compartment apparatus, food pellet was given at one side and 20 Hz light stimulation was applied when mice entered the other side (Fig. 4F). With only mCherry expression in VTA DA neurons, hungry mice spent most of their time in the chamber side with food pellets. However, for the mice with ChR2 expression in VTA DA neurons, the time of hungry mice spent on the food side and non-food (light stimulation) side were not significantly different when activating either VTA DA neurons or dopaminergic axons in the medial NAc (Fig. 4F-4 G, and Figure S6C). We also tested whether mice will trade food for stimulation in a light stimulation magnitude-dependent manner, and observed that mice preferred the food side when activation of VTA DA neurons with 5 Hz light stimulation, and preferred the light stimulation side when activation of VTA DA neurons with 40 Hz light stimulation, but they have no obvious preference when stimulation at 20 Hz (Figure S6D).

Finally, we investigated the positive valence property of activating the VTA-medial NAc-VTA loop circuit with transsynaptic scAAV1-hSyn-Cre injected into VTA, AAV9-DIO-ChR2-mCherry injected into the medial NAc, and optical fiber implanted into VTA in WT mice (Fig. 4H). Similar to activating VTA DA neurons and dopaminergic axons in medial NAc, activating the VTA-medial NAc-VTA loop circuit induced a strong positive valence in normal feeding and fasted mice (Fig. 4I; Figure S6E-F), which was also sufficient to compensate for the hunger-induced food intake (Fig. 4J; Figure S6G). Together, activating the VTA→medial NAc→VTA loop circuit will induce a strong positive valence, which will compensate for the hunger feeling.

3. Discussion

DA signal plays a vital role in regulating reward and motivation behaviors, but the role and neural circuitry mechanisms of VTA DA neurons in regulating food intake remain largely unclear. Here, we found that activating VTA DA neurons will reduce fasted mouse food intake via the positive loop circuit with medial NAc (Fig. 5). Both chemogenetic and optogenetic activation of VTA DA neurons reduce feeding behavior in hungry mice, and refeeding increases the activity of ventral
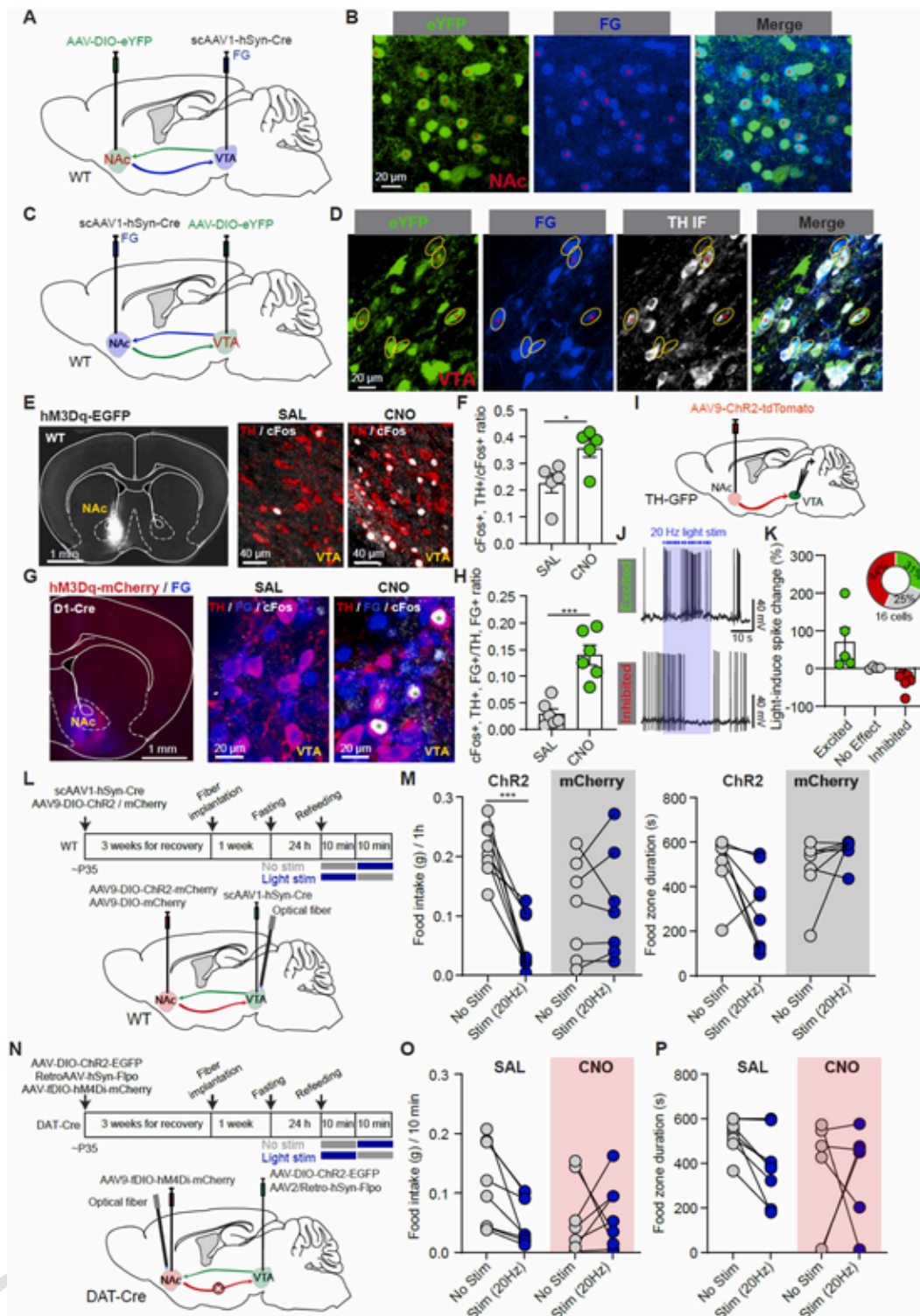
Fig. 3. Ventral VTA DA neurons may form a positive loop with medial NAc in reducing food intake in the 24 h fasted mice. (A) Experimental procedure for tracing the NAc neurons that receive inputs from VTA and also projecting to VTA. (B) Example images show the co-localization between eYFP and FG signals in medial NAc. Red stars indicate eYFP and FG double-positive neurons. (C) Experimental procedure for tracing the VTA neurons that receive inputs from medial NAc and project to medial NAc. (D) Example images show the co-localization between eYFP, FG, and TH signals in VTA. Yellow circles indicate eYFP and FG double positive, and yellow circles with red stars indicate eYFP, FG, and TH triplet-positive neurons. (E) Left: An example image showing hM3Dq-EGFP virus expression in medial NAc of WT mouse. Middle and Right: Images showing cFos expressing in VTA DA neurons (TH IF) when intraperitoneal injection of SAL and CNO. (F) Summary about the ratio of VTA cFos labeled neurons colocalized with TH positive neurons when intraperitoneal injection of SAL and CNO. * $p < 0.05$, unpaired t-test, $n = 5$ mice for each condition. (G) Left: An image showing hM3Dq-mCherry virus and FG expression in medial NAc of D1-Cre mice. Middle and Right: Images showing the colocalization between cFos, TH IF, and FG signals when intraperitoneal injection of SAL and CNO. (H) Summary about the ratio of VTA TH and FG double-labeled neurons colocalized with cFos positive neurons when intraperitoneal injection of SAL and CNO. * ** $p < 0.001$, unpaired t-test, $n = 6$ mice for each condition. (I) Experimental

Fig. 3.—*continued*

strategy to record the response of VTA DA neurons when optically activating medial NAc neuronal axons. (J) Example traces show that activating NAc neuronal axons with 20 s-long 20 Hz blue light stimulation excited (Top) and inhibited (Bottom) VTA DA neurons. (K) Summary about light stimulation-induced activity change of VTA DA neurons. Inset indicates the proportions of excited, no effect, and inhibited neurons when activating NAc neuronal axons. $n = 16$ DA neurons from 4 mice. (L) Experimental procedure for analyzing the effect of activating VTA→medial NAc→VTA circuit on feeding behavior in WT mice. (M) Summary of activating VTA→medial NAc→VTA circuit on food intake (Left) and time spent at the food zone (Right) in 24 h fasted mice. For food intake, RM two-way ANOVA, main effect of light stimulation, $F_{(1, 9)} = 7.225$, $p = 0.0249$; virus expression, $F_{(1, 9)} = 2.669$, $p = 0.1367$ and interaction, $F_{(1, 9)} = 19.21$, $p = 0.0018$. Sidak's multiple comparison test, $* ** p < 0.001$, $* p < 0.05$. For food zone time, RM two-way ANOVA, main effect of light stimulation, $F_{(1, 9)} = 1.874$, $p = 0.2043$; virus expression, $F_{(1, 9)} = 5.577$, $p = 0.0425$ and interaction, $F_{(1, 9)} = 3.352$, $p = 0.1004$. While the pattern of results in the ChR2 group fit within the hypothesis, the study was not sufficiently powered to detect a significant interaction. $n = 8$ and 7 mice for ChR2 and mCherry groups, respectively. (N) Experimental procedure for analyzing the effect of activating dopaminergic axons in medial NAc on feeding behavior with optogenetic method when blocking the VTA-projecting NAc neurons with chemogenetic method. (O) Summary of activating dopaminergic axons in medial NAc on food intake when not blocking (Left) and blocking (Right) the VTA-projecting NAc neurons with chemogenetic method. RM two-way ANOVA, main effect of light stimulation, $F_{(1, 13)} = 3.278$, $p = 0.0934$; CNO, $F_{(1, 13)} = 1.473$, $p = 0.2465$ and interaction, $F_{(1, 13)} = 4.229$, $p = 0.0604$. While the pattern of results in the SAL group fit within the hypothesis, the study was not sufficiently powered to detect a significant interaction. $n = 8$ and 7 mice for SAL and CNO groups, respectively. (P) Same as (O), but for the time spent at the food zone. RM two-way ANOVA, main effect of light stimulation, $F_{(1, 13)} = 5.195$, $p = 0.0402$; CNO, $F_{(1, 13)} = 1.594$, $p = 0.2290$ and interaction, $F_{(1, 13)} = 2.639$, $p = 0.1283$. While the pattern of results in the SAL group fit within the hypothesis, the study was not sufficiently powered to detect a significant interaction.

VTA DA neurons, especially the NAc-projecting VTA DA neurons. Blocking D1 receptors in NAc or inhibiting VTA-projecting NAc neurons are both sufficient to block VTA DA activation-induced food intake reduction. Furthermore, the positive valence induced by activating VTA→medial NAc→VTA loop circuit will compensate for mouse hungry feeling. Collectively, these results suggest the important role of the VTA→medial NAc→VTA circuit in regulating feeding motivation in a hungry state. Our data extend the current knowledge of the role of midbrain DA neurons in modulating food intake and the underlying neural circuitry mechanisms.

Though feeding deficit in DA knockout mice was reversed by DA replenishment (Szczypka et al., 1999), the studies about the role of DA and VTA DA neurons in regulating feeding behavior are inconsistent. Our results suggest that elevating DA level and the activity of VTA DA neurons in adult mice will reduce food intake in a hungry state (Fig. 1), which seems to be controversial with the effects of DA replenishment in DA knockout mice (Szczypka et al., 1999) and metabolic signals, including leptin, insulin, and ghrelin (Abizaid et al., 2006; Hommel et al., 2006; Mebel et al., 2012). Compared with our study, these studies directly manipulated VTA DA neurons (Abizaid et al., 2006; Hommel et al., 2006; Mebel et al., 2012; Szczypka et al., 1999), and the effects of DA neurons in other brain regions or VTA non-DA neurons may override the function of VTA DA neurons. For example, activating VTA GABA neurons with 20 Hz light stimulation will increase the standard food intake in the 24 h fasted mice in our study (Figure S3F). Van Zessen and colleagues found that activation of VTA GABA neurons by continuous light stimulation disrupted reward consummatory behavior when mice were food restricted to 85%– 90% of their free-feeding bodyweight (Van Zessen et al., 2012). However, another study showed that both standard chow and high fat/sugar chow increase the activity of VTA GABA neurons, and activation of VTA GABA neurons with 10 Hz light stimulation will increase the biting of standard food and the consumption of high fat/sugar chow in the stated mice, but reduce the intake of standard chow, not the high fat chow, in the 12 h food-deprived mice (Chen et al., 2020). Different feeding states and different optogenetic activation patterns may induce these diverse effects of activating VTA GABA neurons on feeding behavior in different studies. In addition, VTA is heterogeneity in neural connectivity and function (Morales and Margolis, 2017) and VTA GABA neurons in different spatial locations have biased input patterns (Beier et al., 2019), therefore activating GABA neurons in different subregions of VTA may also contribute to the inconsistent results of feeding behaviors in different studies. We confirmed that activating VTA DA neurons reduces mouse food intake through several different experiments. Acute chemogenetical or optogenetic activation, but not inhibition, of VTA DA neurons reliably reduced mouse food intake after 24 h fasting. Meanwhile, long-term activation of VTA DA neurons was sufficient to reduce both mouse body weight and food intake. Other recent studies also observed that optoge-

netic activation of VTA DA neuronal projections reduced food intake (Cai et al., 2022; Han et al., 2021). In our long-term chemogenetic activation experiment, although mouse weight stably decreased with CNO administration, mice only significantly reduced the food intake at first several days. Two possible reasons may contribute to this phenomenon. Firstly, CNO was intraperitoneally injected three times per day with 8-h interval in our study and CNO-induced activation will decay over time. The effect of systemic CNO administration on neuronal activity can last ~9 h, but reaches the peak after 45–50 min (Alexander et al., 2009). Chemogenetic activation of VTA DA neurons may be not strong enough to compensate for the hungry-induced feeding at several hours after CNO injection, and mice may shift the feeding time after chemogenetic activation for several days. Secondly, chemogenetic activation efficiently reduced body weight during CNO administration and our previous study showed that activation of VTA DA neurons will increase mouse motor activity (Tong et al., 2023), which will elevate energy expenditure. Motor activity-induced energy expenditure may induce more food intake, which will override the food intake reduction directly induced by activating VTA DA neurons.

Given the diversity of VTA DA neurons in functions and projections (Morales and Margolis, 2017), we explored the distribution and projection of VTA DA neurons related to feeding behavior. Our results showed that DA neurons in ventral VTA, especially neurons projecting to the medial NAc, are activated after refeeding in 24 h fasted mice, and activating DA axons in medial NAc reliably reduced mouse food intake in a hungry state. Activating VTA DA neuronal fibers in LH also tended to reduce mouse food intake, but direct activation of VTA DA neurons projecting to LH did not have a significant change. The VTA DA neuronal axons projecting to NAc will pass through the LH, and previous study showed that activating the fibers of passage may induce behavior change (Marino et al., 2020), so we infer that food intake reduction induced by optogenetic activation of VTA DA neuronal fibers in LH may reduce food intake by activating NAc-projecting VTA DA neuronal axons. Previous studies reported that activating the projection of VTA DA neurons to NAc did not affect feeding behavior (Boekhoudt et al., 2017; Han et al., 2021), and restoration of DA production in the NAc did not rescue the feeding behavior in the DA-deficient mice (Szczypka et al., 2001). NAc are divided into the medial shell, lateral shell, and core based on anatomy and functions. Silencing medial NAc, but not lateral NAc was reported to promote food intake (Basso and Kelley, 1999). The anterior paraventricular nucleus of the thalamus (aPVT) and prefrontal cortex (PFC) target distinct areas of NAc to oppositely modulate high fat intake (Christoffel et al., 2021). The activity of medial NAc D1 neurons was inhibited during food consumption, and activating medial NAc D1 neurons rapidly stopped feeding (O'Connor et al., 2015). Despite activating the projection from medial NAc to VTA induces a general state of behavioral suppression that is not specific to reward or aversion (Yang et al., 2018), the activity of VTA DA terminals in the
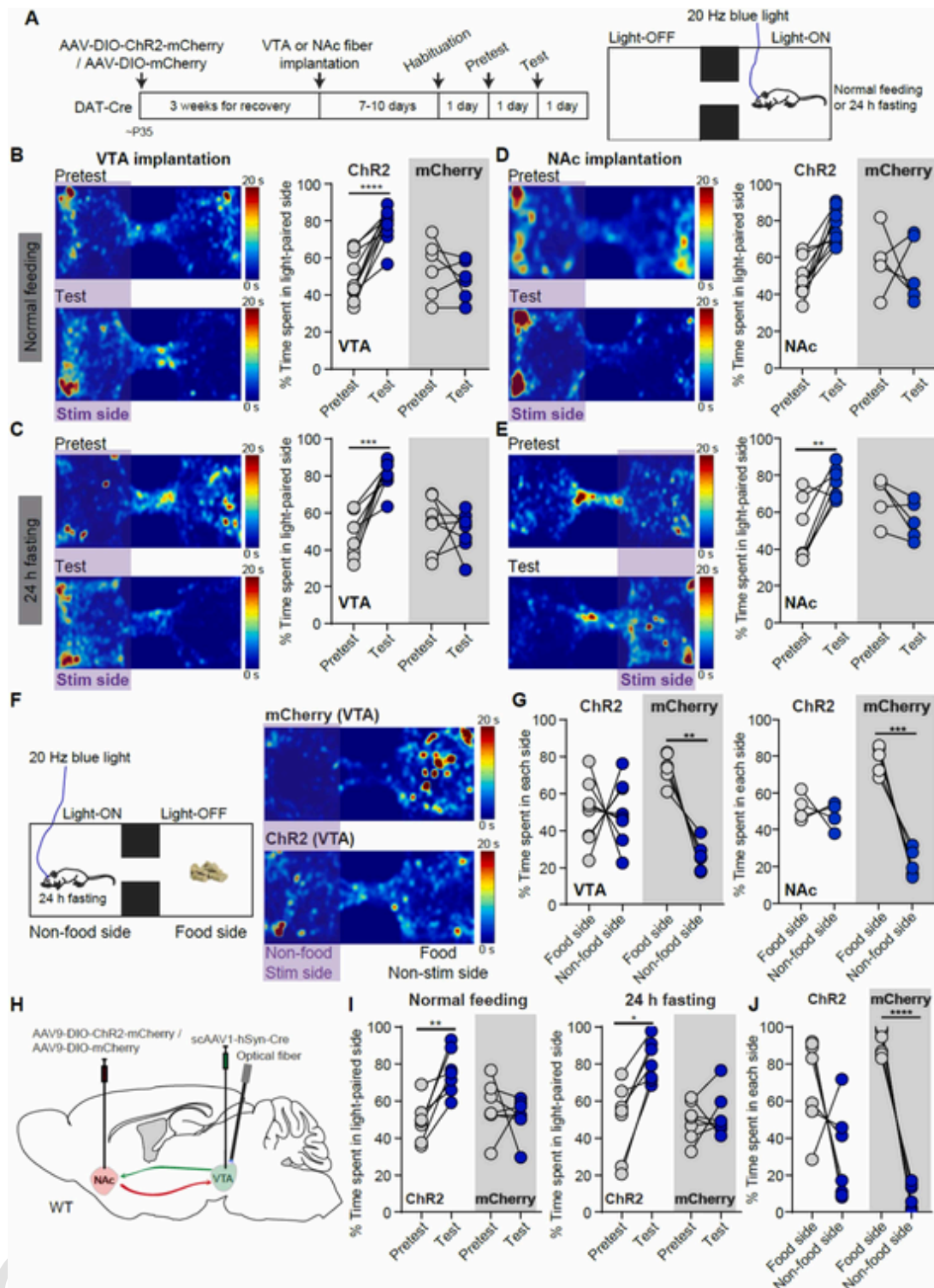
Fig. 4. Activating the VTA→medial NAc→VTA loop circuit will compensate for the hunger-induced food intake. (A) Left: Experimental procedure to investigate the positive valence property by activating VTA DA neurons or dopaminergic axons in medial NAc. Right: The three-compartment apparatus for real-time place preference behavior test. (B) Left: The time heat maps of one example VTA fiber implanted mouse spent at stimulation and non-stimulation sides in the pretest (Top) and test (Bottom) stages. Right: Summary of the percentage of time spent on the light-paired side in the pretest and test stages in normal feeding mice with ChR2-mCherry and mCherry viruses expressed in VTA DA neurons and optical fiber implanted into VTA. RM two-way ANOVA, main effect of light stim, $F_{(1, 15)} = 10.67$, $p = 0.0052$; virus expression, $F_{(1, 15)} = 7.418$, $p = 0.0157$ and interaction, $F_{(1, 15)} = 25.39$, $p = 0.0001$. Sidak's multiple comparison test, $****p < 0.0001$, $n = 11$ and 6 mice for ChR2 and mCherry groups. (C) Same as (B), but for mice at 24 h fasting state. RM two-way ANOVA, main effect of light stim, $F_{(1, 13)} = 8.928$, $p = 0.0105$; virus expression, $F_{(1, 13)} = 14.16$, $p = 0.0024$ and interaction, $F_{(1, 13)} = 14.34$, $p = 0.0023$. Sidak's multiple comparison test, $***p < 0.001$, $n = 8$ and 7 mice for ChR2 and mCherry groups. (D) Same as (B), but for normal feeding mice with optical fiber implanted into the medial NAc. RM two-way ANOVA, main effect of light stim, $F_{(1, 10)} = 1.862$, $p = 0.2024$; virus expression, $F_{(1, 10)} = 3.37$, $p = 0.1007$ and interaction, F

Fig. 4.—*continued*

(1, 10) = 4.366, p = 0.0632. While the *p*attern of results in the ChR2 group fit within the hypothesis, the study was not sufficiently powered to detect a significant interaction. n = 10 and 5 mice for ChR2 and mCherry groups. (E) Same as (D), but for 24 h fasted mice with optical fiber implanted into the medial NAc. RM two-way ANOVA, main effect of light stim, $F_{(1, 10)}$ = 2.270, p = 0.1628; virus expression, $F_{(1, 10)}$ = 0.0145, p = 0.9066 and interaction, $F_{(1, 10)}$ = 17.51, p = 0.0019. Sidak's multiple comparison test, $**p < 0.01$, n = 7 and 5 mice for ChR2 and mCherry groups. (F) Left: The experimental paradigm to measure real-time place preference in 24 h fasted mice with light stimulation when on the non-food side and without stimulation when on the food side. Right: Heat map of time spent at each side in the real-time place preference for example mice with mCherry (Top) and ChR2-mCherry (Bottom) expressed in VTA DA neurons and optical fiber implanted into VTA. (G) Summary of the percentage of time spent at food side and non-food side in the real-time place preference when activating VTA DA neurons (Left) and dopaminergic axons in medial NAc (Right). For VTA, RM two-way ANOVA, main effect of light stim, $F_{(1, 12)}$ = 41.92, $p < 0.0001$; place, $F_{(1, 12)}$ = 9.989, p = 0.0082 and interaction, $F_{(1, 12)}$ = 10.18, p = 0.0078. For NAc, RM two-way ANOVA, main effect of light stim, $F_{(1, 7)}$ = 29.46, p = 0.0010; place, $F_{(1, 7)}$ = 36.43, p = 0.0005 and interaction, $F_{(1, 7)}$ = 26.57, p = 0.0013. Sidak's multiple comparison test, $**p < 0.01$, $***p < 0.001$, n = 8 and 6 mice for VTA fiber implanted ChR2 and mCherry groups, n = 4 and 5 mice for NAc fiber implanted ChR2 and mCherry groups. (H) Experimental strategy to activate VTA-medial NAc-VTA loop circuit. (I) Summary about the percentage of time spent on the light-paired side in the pretest and test stages in normal feeding (Left) and 24 h fasted (Right) mice when activating the VTA-medial NAc-VTA loop circuit. For normal feeding, RM two-way ANOVA, main effect of light stim, $F_{(1, 12)}$ = 4.743, p = 0.0501; virus expression, $F_{(1, 12)}$ = 4.272, p = 0.0610 and interaction, $F_{(1, 12)}$ = 9.792, p = 0.0087. For 24 h fasting, RM two-way ANOVA, main effect of light stim, $F_{(1, 12)}$ = 13.48, p = 0.0032; virus expression, $F_{(1, 12)}$ = 6.920, p = 0.0219 and interaction, $F_{(1, 12)}$ = 9.937, p = 0.0083. Sidak's multiple comparison test, $*p < 0.05$, $**p < 0.01$, n = 7 and 7 mice for ChR2 and mCherry groups. (J) Summary about the *p*ercentage of time spent at the food side and non-food side in the real-time place preference when activating the VTA-medial NAc-VTA loop circuit. RM two-way ANOVA, main effect of light stim, $F_{(1, 12)}$ = 0.6, p = 0.4536; place, $F_{(1, 12)}$ = 43.56, $p < 0.0001$ and interaction, $F_{(1, 12)}$ = 4.972, p = 0.0456. Sidak's multiple comparison test, $****p < 0.0001$, n = 7 and 7 mice for ChR2 and mCherry groups.
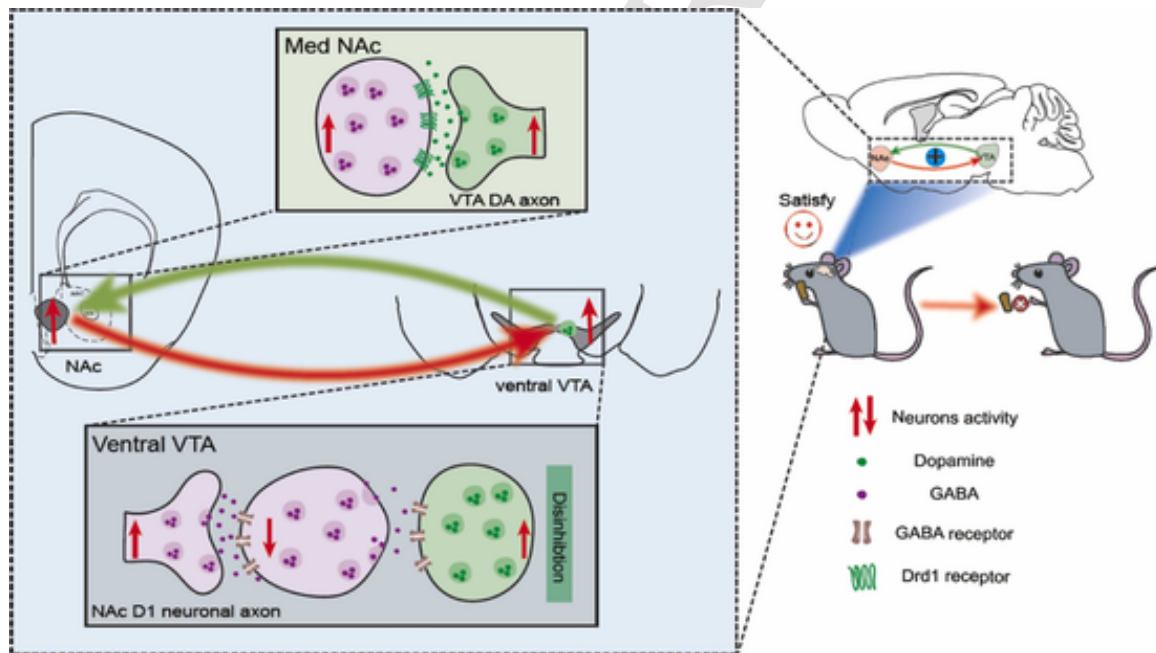
Fig. 5. Schematic depiction of the main findings in this study. Activating ventral VTA DA neurons reduces mouse food intake in a hungry state via projecting to medial NAc and activating D1 receptors, and NAc D1 neurons then project back to ventral VTA to disinhibit VTA DA neurons. The possible VTA→medial NAc→VTA dopaminergic loop encodes positive valence, which will resist the hungry feeling.

ventral part and dorsal part of medial NAc exhibited opposite changes by unexpected aversive stimulation (de Jong et al., 2019), which suggests the functional heterogeneity of VTA DA signal across dorsal-ventral medial NAc. Medial NAc contains both types of the reward-excited and reward-inhibited neurons (Chen et al., 2023). In this study, we observed that activating the projection of VTA to medial NAc reduces the hungry-induced feeding behavior, which can be blocked by inhibiting medial NAc D1 neurons. Therefore, we infer that VTA DA neurons may activate the reward-excited neurons in the medial NAc to promote reward and reduce food intake.

Medial NAc D1 neurons can project to ventral VTA and disinhibit VTA DA neurons via VTA GABA neurons (Bond et al., 2020; Edwards et al., 2017; Liu et al., 2022; Yang et al., 2018). Both VTA DA and non-DA neurons form bi-directional connections with medial NAc (Fig. 3), which is consistent with previous studies (Beier et al., 2015; Edwards et al., 2017). The projection of medial D1 neurons to VTA is found to suppress food consumption (Bond et al., 2020). Our study found that acti-

vating VTA→NAc→VTA recurrent loop will reduce the food intake, but it is a pity that we are not able to directly investigate whether VTA DA and GABA neurons are both involved or not in the food intake reduction because of the technical limitations. However, we think the projection of VTA DA neurons to the medial NAc is involved in the food intake reduction induced by activating the VTA→NAc→VTA recurrent loop based on the following reasons: 1) Activating VTA DA neurons and GABA neurons have opposite effects on food intake, and activation of the VTA→NAc→VTA recurrent loop has a similar effect on food intake as activating VTA DA neurons or dopaminergic axons in medial NAc; 2) Activating medial NAc D1 neurons increases the cFos expression in the ventral VTA DA neurons which project to the medial NAc; 3) Inhibiting the VTA-projecting neurons in NAc can block the food intake reduction induced by activating dopaminergic projection from VTA to the medial NAc.

Previous studies showed that stimulus-induced positive/negative valence can modulate hungry animals' desire for food (Cai et al., 2022;

Imoto et al., 2021; Sternson, 2016). VTA DA signal is suggested to encode positive valence, and activating DA axons in NAc will induce place preference (Mahadevia et al., 2021). In our study, we observed that activating VTA DA neurons or DA axons in medial NAc induces a strong positive valence in either a normal feeding state or 24 h fasting state, which will override the desire for food consumption in a hungry state. High frequency activating the projection of VTA DA neurons to the dorsal raphe nucleus (DRN) also induces positive valence and reduces food intake (Cai et al., 2022). Previous studies also showed that inhibition of VTA DA neurons reliably induces aversive behaviors in the place preference test (Chang et al., 2015; Danjo et al., 2014; Ilango et al., 2014; Tan et al., 2012). Considering activation of VTA DA neurons reduced mouse food intake, we expected that inhibition of VTA DA neurons might increase food intake. However, in our both chemogenetic and optogenetic inhibition experiments, inhibiting VTA DA neurons did not significantly change food intake and the time spent at the food zone, so we did not further explore the effects of optogenetic inhibiting VTA DA neurons in other experiments, including the place preference tests. We infer that although inhibition of VTA DA neurons will induce aversive avoidance, this aversive behavior may have weak effect on the hungry-induced homeostatic food intake. Considering the obesity prevalence, developing a strategy to activate medial NAc or DRN-targeting VTA DA neurons may be efficient to reduce body weight.

In summary, the effects of VTA DA signal on feeding behavior are complex. In this study, we dissected the anorexigenic effect of the VTA→medial NAc→VTA loop circuit and proved the positive valence encoded by this circuit can compensate for food intake in hungry mice. These findings not only uncover a new DA circuit in regulating food intake but also suggest the possible translational value of elevating VTA DA-related positive valence in losing weight.

4. Material and methods

4.1. Mouse strains and genotyping

All animal procedures were approved by the Fudan University Animal Care and Use Committee. Adult mice (5–12 weeks) were group-housed on a 12:12 light-dark cycle (8 am light-ON and 8 pm light-OFF) with ad libitum access to standard chow diet and water in the room that was controlled for temperature and humidity unless otherwise noted. Mouse lines used in this study including: C57BL/6 mice were obtained from Shanghai Model Organisms Center; B6. SJL-Slc6a3 [tm1.1(cre)Bkmn]/J mice (DAT-Cre, #006660, Jackson Laboratory), which express Cre recombinase under the control of DA transporter promoter, were used to target VTA DA neurons (Bäckman et al., 2006); B6. FVB-Tg(Slc32a1-Cre)2.1Hzo/FrkJ mice (Vgat-Cre, #017535, Jackson Laboratory) were used to express Cre recombinase in GABAergic neurons; Slc17a6 [tm2(cre)Lowl]/J mice (Vglut2-Cre, #016963, Jackson Laboratory) were used to express Cre recombinase in glutamatergic neurons; Tg(Drd1-Cre)EY262Gsat/Mmucd mice (D1-Cre, 034258-UCD, MMRRC) express Cre recombinase in DA Drd1 receptor-positive neurons (Gong et al., 2007) and Tg(Th-EGFP)DJ76Gsat mice (TH-GFP, MGI: 3846686) were used to label VTA dopamine neurons. The B6. Cg-Gt(ROSA)26Sor[tm3(CAG-EYFP)Hze]/J (Ai3, #007903, Jackson Laboratory) reporter strain was crossed with GAD-Cre mice (#010802, Jackson Laboratory) to visualize GABAergic neurons. Mouse genotyping were conducted following standard procedures on the Jackson Lab website or MMRRC website. Mice heterozygous for Cre were used for experiments. Because we did not observe any sex differences, data from males and females were analyzed together.

4.2. In vivo stereotaxic intracranial injection

Mice aged 7–8 weeks were anesthetized with 0.5%– 2% isoflurane, and placed in a stereotaxic apparatus (E07370–005, RWD). For virus injections, recombinant AAVs were delivered into brain regions by a microsyringe pump controller (NanoJect III, Drummond Scientific Company) at a volume of 50–180 nL with a flow rate of 1 nL/s. Injection pipette was left at the injection site for 10–15 min after viral delivery to assure adequate viral delivery. The following coordinates were used: VTA (2.8 mm posterior to bregma, 0.3 mm lateral to the midline, 4.6 and 4.8 mm below the pia), medial NAc (1.6 mm anterior to bregma, 0.9 mm lateral to the midline, 4.5 mm below the pia), lateral NAc (1.6 mm anterior to bregma, 1.5 mm lateral to the midline, 4.6 mm below the pia), mPFC (1.9 mm anterior to bregma, 0.3 mm lateral to the midline, 2.0 mm below the pia), LS (0.6 mm anterior to bregma, 0.3 mm lateral to the midline, 3.0 mm below the pia), LH (0.4 mm posterior to bregma, 1.2 mm lateral to the midline, 5.0 mm below the pia), amygdala (1.2 mm posterior to bregma, 3.2 mm lateral to the midline, 4.6 mm below the pia), vHipp (2.8 mm posterior to bregma, 2.8 mm lateral to the midline, 3.9 mm below the pia), PBN (4.4 mm posterior to bregma, 1.2 mm lateral to the midline, 3.1 mm below the pia). Coordinates were slightly adjusted based on mouse age and brain size.

The following AAV viruses were used in this study: AAV2-hSyn-DIO-hM3D(Gq)-mCherry (4.6×10^{12} vector genomes/mL, Taitool), AAV9-hSyn-DIO-hM4D(Gi)-mCherry (4.55×10^{12} vector genomes/mL, Taitool), AAV9-hSyn-DIO-mCherry (4.2×10^{12} vector genomes/mL, Taitool), AAV9-hEF1a-DIO-hChR2(H134R)-mCherry (3.4×10^{12} vector genomes/mL, Taitool), AAV9-hEF1a-DIO-eNpHR3.0-EYFP (1.48×10^{12} vector genomes/mL, Taitool), RetroAAV-CAG-Flex-Flpo (1.66×10^{13} vector genomes/mL, Taitool), AAV9-hEF1a-fDIO-hChR2(H134R)-EYFP (1.65×10^{12} vector genomes/mL, Taitool), AAV9-EF1a-DIO-EYFP (2.93×10^{12} vector genomes/mL, BrainVTA), 2% Fluoro-Gold (FG), scAAV1-hsyn-Cre (1.18×10^{13} vector genomes/mL, Taitool), rAAV-hSyn-hM3D(Gq)-EGFP (1.19×10^{12} vector genomes/mL, BrainVTA), AAV9-CAG-hChR2-H134R-tdTomato (1.36×10^{12} vector genomes/mL, Taitool), rAAV-EF1α-DIO-hChR2(H134R)-EYFP (1.08×10^{12} vector genomes/mL, BrainVTA), RetroAAV-hSyn-Flpo-pA (1.21×10^{13} vector genomes/mL, Taitool), AAV2/9-hEF1a-fDIO-hM4D(Gi)-mCherry (1.05×10^{12} vector genomes/mL, Taitool).

4.3. Optical fiber and cannula implantation

For in vivo photostimulation experiments, an optical fiber (200 μm, 0.37 NA, Newdoon) was implanted into the related brain region VTA (2.8 mm posterior to bregma, 0.3 mm lateral to the midline, 4.2 below the pia), medial NAc (1.6 mm anterior to bregma, 0.9 mm lateral to the midline on one side and 1.6 mm lateral to the midline at 10° angle from the midline on the other side, 4.0 mm below the pia), LS (0.6 mm anterior to bregma, 0.3 mm lateral to the midline, 2.7 mm below the pia), LH (0.4 mm posterior to bregma, 1.2 mm lateral to the midline, 4.7 mm below the pia), using stereotaxic apparatus at least 3 weeks after viral injection surgery. For drug microinjection, mice were implanted with a stainless-steel guide cannula (26-gauge) bilaterally above the NAc (1.6 mm anterior to bregma, 1.0 mm lateral to the midline, and 3.5 mm below the pia). Stainless dummies were inserted into the guide cannula to prevent the guide cannula from clogging. Dental cement was used to secure optical fibers and cannula to the skull. At least 1 week after fiber or cannula implantation surgery, mice were anesthetized with 0.5%– 1% isoflurane, vehicle or drug (750 ng/μl SCH23390) was delivered into the NAc via an injection cannula that extended 1.0 mm beyond the tip of the guide cannula (Tong et al., 2023). A volume of 650 nl vehicle or drug was injected over a 5-min period. The injection cannula was kept in the injection place for an additional 5 min to minimize the drug leaking. Behavioral tests were conducted around 40 min after microinjection. Brains were sectioned to verify the optical fiber and cannula location and injection site after finishing all the behavioral tests (Figure S7). Mice with wrong implantation locations were excluded from analyses.

4.4. Acute slice preparation and electrophysiological recording

Acute brain slices were prepared according to the previously described (S. Chen et al., 2022; Tong et al., 2023; Xiao et al., 2018). Mice were anesthetized by isoflurane and transcardially perfused with the ice-cold, oxygenated artificial cerebrospinal fluid (ACSF) (in mM): 127 NaCl, 2.5 KCl, 25 NaHCO$_3$, 1.25 NaH$_2$PO$_4$, 2 CaCl$_2$, 1 MgCl$_2$, and 25 Glucose (Osmolarity ~310 mOsm/L). Mouse brain was quickly removed and immersed in a slicing chamber containing ice-cold ACSF, bubbled with 95% O$_2$ / 5% CO$_2$. Coronal slices with ~ 250 μm thickness were cut on a slicer (Vibratome 1000PLUS), and slices were incubated in the oxygenated ACSF for ~30 min at 34 °C before recording.

Slices were transferred to a recording chamber with oxygenated ACSF perfusion at a flow rate of 1.5–2 mL/min, and the temperature was maintained at ~ 30 °C during recording via a feedback in-line heater (TC-324 C; Warner Instruments, Hamden, CT). Fluorescence-labeled neurons were identified using microscopy, and VTA DA and non-DA neurons were discriminated by the GFP expression with TH-GFP transgenic mice. In both the cell-attached model and current-clamp whole-cell model, the spontaneous action potential was recorded with the internal solution consisting of (in mM): 135 K-gluconate, 4 KCl, 10 HEPES, 10 Na-phosphocreatine, 4 MgATP, 0.4 Na$_2$GTP, and 1 EGTA (with pH 7.2 – 7.3, and osmolarity ~295 mOsm/L). For optogenetic activation or inhibition, blue-light or yellow-light stimulation was delivered at the recording site through a 40 × water objective with an X-Cite 110LED (Excelitas Canada Inc.), filtered with a GFP filter cube and triggered by Master-8 (A.M.P.I., Israel). Recordings were made using a 700B amplifier, data were digitized at 10 kHz and filtered at 4 kHz, and collected using pCLAMP software (Molecular Devices).

4.5. Tissue processing, immunohistochemistry and imaging

Mice were anesthetized with isoflurane and perfused transcardially with 4% paraformaldehyde (PFA) in 0.1 M phosphate-buffered saline (PBS). Mouse brains were dissected from the skull and post-fixed in 4% PFA at 4 °C for 1–2 days. After washing with PBS, brains were coronally sectioned at 50–60 μm on a vibratome (VT1200, Leica, Germany). Every 3rd brain slices were chosen and pretreated in 0.2% Triton-X10 in PBS for 1 h at room temperature (RT), then blocked with 0.05% Triton-X100, 10% bovine serum albumin (BSA) in PBS for ~1 h at RT and rinsed in PBS. Brain slices were transferred into primary antibody solution (Rabbit anti-TH, 1:1000, AB152, Millipore; Mouse anti-TH, 1:1000, AB129991, Abcam; Rabbit anti-cFos, 1:1000, Cell Signaling) in PBS with 0.2% Triton-X100 and incubated overnight at 4 °C. Tissues were rinsed in PBS three times, and incubated with secondary antibody solution (Goat anti-Rabbit 594, 647, Goat anti-Mouse 647, 1:1000, Life Technologies) in PBS for 2 h at RT, then rinsed and mounted onto slides, dried and covered under glycerol: TBS (3:1) with Hoechst 33342 (1:1000, ThermoFisher Scientific). Sections were imaged with an Olympus VS120 slide scanning microscope with 10 × objectives. Confocal images were acquired with a Nikon A1 confocal laser scanning microscope with 20 × objectives. Images were analyzed in ImageJ (FIJI).

4.6. Behavioral tests

Feeding behavioral tests were conducted between 10:00 am – 10:00 pm. Mice were habituated in the behavior testing room for at least 1 h before all the experimental tests. Mice were randomly assigned to be control and experimental groups. If not specifically stated, behavioral tests were performed with light-on. Behavioral apparatuses were cleaned and wiped with 75% ethanol to remove odor clues left by the previous subject between trials. Only one behavioral test was conducted each time for all the pharmacological, optogenetic, and chemo-

genetic manipulations, and the interval between different tests was at least 3 days.

For the chemogenetic manipulation, normal feeding or fasted mice were separately transferred to a clear cage and allowed to habituate the cage for ~1 h. Clozapine-n-oxide (CNO, 2 mg/kg) or saline (SAL) was intraperitoneally (i.p.) administrated ~30 min before refeeding the food intake test. A weighted standard laboratory chow or High fat (HF) diet was placed in the cage. The amount of food intake within 1 h was measured. Saline and CNO were administered in a crossover order with at least a 5 days-interval. The chronic chemogenetic manipulation was performed as previously described (Krashes et al., 2011). After the functional expression of chemogenetic viruses, mice were singly housed with a continuous intraperitoneal injection of saline for 7 days to adaptive the daily injection. Mice were randomly divided into SAL and CNO groups, and CNO (2 mg/kg) or saline was i.p. administrated three times per day for 7 days. Mouse body weight and food intake were monitored every day.

For the optogenetic manipulation, 10-ms blue laser pulses (intensity power at fiber tip was ~10 mW) with the frequency of 5 Hz, 10 Hz, 20 Hz, and 40 Hz were generated from a 473-nm blue solid-state laser, or the 10-min continuous yellow light (intensity power at fiber tip was ~10 mW) were generated from a 593-nm blue solid-state laser, and stimulation patterns were controlled by the DigiStim (Thinker Tech Nanjing Bioscience Inc). The day before the first behavioral test, mice were connected to the patch cord and habituated to the optogenetic system for at least 15 min. The food intake measurement test of 24 h fasted mice was divided into three stages. Mice were first habituated to behavioral apparatus with two glass dishes on different corners for 10 min. In the second stage, a weighed standard laboratory chow was placed into a glass dish randomly. In the third stage, another weighed standard laboratory chow was placed into the other side glass dish. The glass dishes were cleaned and wiped with 75% ethanol. In the latter two stages, to exclude the effect induced by different degrees of hunger, 10-min optogenetic stimulation in some mice was given immediately after habituation followed with 10 min light stimulation off (light stimulation to without light stimulation protocol), and for the other mice stimulation was given at the third stage of the test (without light stimulation to light stimulation protocol). After 10 min feeding, the chow and all food debris were collected to weigh. The food intake and time spent in the food zone with and without light stimulation were measured. The food zone was defined as a square enclosing the circular glass dish with the diameter length of the glass dish as the side length. Food zone duration was calculated after mouse trajectories detected with the Toxtrac software (https: //toxtrac.sourceforge.io). The feeding time measurement test of 24 h fasted mice was divided into four stages. The subject mice were placed in a 5 L (19 cm [D] x 26 cm [H]) clean clear glass beaker after gently connecting to the fiber-optic patch. After 5 min habituation, a normal laboratory chow was placed in a glass dish, followed by a 10 min light stimulation off to 10 min 20 Hz 10-ms optogenetic light stimulation, then to 10 min light stimulation off protocol. The whole process is recorded from the side of the beaker to measure the feeding time of mice.

The real-time place preference test was conducted to evaluate the positive or negative valence. The experimental protocol for normal feeding mice or 24 h fasted mice was performed as previously described with some adjustments (Mahadevia et al., 2021). A three-compartment apparatus consists of two main compartments (20 cm [W] x 20 cm [L] x 30 cm [H]) with distinct visual and tactile cues and one neutral connecting compartment (10 cm [W] x 10 cm [L] x 30 cm [H]). The whole experiment lasted three days. On the first day, gently placed each mouse into the neutral compartment after connecting to the fiber-optic patch. The mouse was allowed to explore freely 15 min to habituate the apparatus. On the second day or the pretest day, the mouse was allowed to explore the apparatus for 30 min with the patch connected but without stimulation, and the video was recorded to calculate the initial

place preference for the two main compartments. After the pretest, mice were deprived of food for 24 h if mentioned. On the third day or the test day, the mouse was allowed to explore for 30 min, during which a 473-nm 20 Hz 10-ms laser stimulation was given when the mouse entered the light-paired side. The stimulation was terminated when the mouse left the randomly assigned stimulation side. The proportion of time spent on the light-paired side was defined as the time stayed on the light-paired side divided by the sum of the time stayed on both stimulation and non-stimulation sides. Mice with an initial preference of more than 80% during the pretest were excluded.

To access the influence of valence induced by the optogenetic stimulation on the hungry feeling in 24 h fasted mice, normal chow pellets were randomly placed in one chamber and the other chamber was assigned as the stimulation side (Cai et al., 2022). The proportion of time spent on the light-paired side (non-food side) was defined as the time stay on the assigned light-paired side divided by the sum of the time stay on the stimulation side and non-stimulation side (food side).

4.7. Quantification and Statistical Analysis

In our study, no statistical method was used to pre-determine sample sizes, and the sample sizes were determined based on previous studies conducted in the same field. All behavioral and electrophysiological recording data analyses were performed using MATLAB (Mathworks), pClamp10 (Molecular Devices), or GraphPad Prism (GraphPad). All image analyses were carried out in ImageJ (FIJI, NIH). Whenever possible, data were analyzed blind to condition. Normality was assessed by the Shapiro-Wilk test. For normal distributions, homoscedasticity was assessed by F-test using GraphPad Prism. For homogeneous variances, two-tailed t-test and paired/unpaired t-test were used for single and paired comparisons, and one-way ANOVA followed by post hoc Tukey's test or two-way ANOVA followed by Sidak's multiple comparison test was used for multiple comparisons. When variances were not homogeneous, a *t*-test with Welch's correction was used. For data that were not normally distributed, Wilcoxon signed rank test, Mann-Whitney test or Wilcoxon matched-pairs signed rank test was used for single and paired comparisons, and Friedman test followed by post hoc Dunn's test was used for multiple comparisons. $p < 0.05$ was considered statistically significant.

Uncited references

.

CRediT authorship contribution statement

L.X., X.C., and Q.P.T designed the experiments. H.X. and C.T.X. performed *ex vivo* electrophysiology and data analyses, X.C. and Q.P.T. carried out stereotaxic surgery. X.C. and Q.P.T. carried out behavioral experiments and analyses. L.X. and X.C. wrote the paper, with the contributions from all authors.

Declaration of Competing Interest

The authors declare no competing interests.

Data Availability

Data will be made available on request.

Acknowledgments

References

Abizaid, A., Liu, Z., Andrews, Z.B., Shanabrough, M., Borok, E., Elsworth, J.D., Roth, R.H., Sleeman, M.W., Picciotto, M.R., Tschöp, M.H., Gao, X., Horvath, T.L., 2006. Ghrelin modulates the activity and synaptic input organization of midbrain dopamine neurons while promoting appetite. J. Clin. Invest 116, 3229–3239. https://doi.org/10.1172/JCI29867.In.

Alcantara, I.C., Tapia, A.P.M., Aponte, Y., Krashes, M.J., 2022. Acts of appetite: neural circuits governing the appetitive, consummatory, and terminating phases of feeding. Nat. Metab. https://doi.org/10.1038/s42255-022-00611-y.

Alexander, G.M., Rogan, S.C., Abbas, A.I., Armbruster, B.N., Pei, Y., Allen, J.A., Nonneman, R.J., Hartmann, J., Moy, S.S., Nicolelis, M.A., McNamara, J.O., Roth, B.L., 2009. Remote control of neuronal activity in transgenic mice expressing evolved G protein-coupled receptors. Neuron 63, 27–39. https://doi.org/10.1016/j.neuron.2009.06.014.

Bäckman, C.M., Malik, N., Zhang, Y., Shan, L., Grinberg, A., Hoffer, B.J., Westphal, H., Tomac, A.C., 2006. Characterization of a mouse strain expressing Cre recombinase from the 3' untranslated region of the dopamine transporter locus. Genesis 44, 383–390. https://doi.org/10.1002/dvg.20228.

Basso, A.M., Kelley, A.E., 1999. Feeding induced by GABA(A) receptor stimulation within the nucleus accumbens shell: regional mapping and characterization of macronutrient and taste preference. Behav. Neurosci. 113, 324–336. https://doi.org/10.1037/0735-7044.113.2.324.

Beier, K.T., Steinberg, E.E., DeLoach, K.E., Xie, S., Miyamichi, K., Schwarz, L., Gao, X.J., Kremer, E.J., Malenka, R.C., Luo, L., 2015. Circuit architecture of VTA dopamine neurons revealed by systematic input-output mapping. Cell 162, 622–634. https://doi.org/10.1016/j.cell.2015.07.015.

Beier, K.T., Gao, X.J., Xie, S., DeLoach, K.E., Malenka, R.C., Luo, L., 2019. Topological organization of ventral tegmental area connectivity revealed by viral-genetic dissection of input-output relations. Cell Rep. 26, 159–167.e6. https://doi.org/10.1016/j.celrep.2018.12.040.

Boekhoudt, L., Roelofs, T.J.M., De Jong, J.W., De Leeuw, A.E., Luijendijk, M.C.M., Wolterink-Donselaar, I.G., Van Der Plasse, G., Adan, R.A.H., 2017. Does activation of midbrain dopamine neurons promote or reduce feeding? Int. J. Obes. 41, 1131–1140. https://doi.org/10.1038/ijo.2017.74.

Bond, C.W., Trinko, R., Foscue, E., Furman, K., Groman, S.M., Taylor, J.R., DiLeone, R.J., 2020. Medial nucleus accumbens projections to the ventral tegmental area control food consumption. J. Neurosci. 40, 4727–4738. https://doi.org/10.1523/jneurosci.3054-18.2020.

Cai, X., Liu, Hailan, Feng, B., Yu, M., He, Yang, Liu, Hesong, Liang, C., Yang, Y., Tu, L., Zhang, N., Wang, L., Yin, N., Han, J., Yan, Z., Wang, C., Xu, P., Wu, Q., Tong, Q., He, Yanlin, Xu, Y., 2022. A D2 to D1 shift in dopaminergic inputs to midbrain 5-HT neurons causes anorexia in mice. Nat. Neurosci. 25, 646–658. https://doi.org/10.1038/s41593-022-01062-0.

Chang, C.Y., Esber, G.R., Marrero-Garcia, Y., Yau, H.J., Bonci, A., Schoenbaum, G., 2015. Brief optogenetic inhibition of dopamine neurons mimics endogenous negative reward prediction errors. Nat. Neurosci. 19, 111–116. https://doi.org/10.1038/nn.4191.

Chen, G., Lai, S., Bao, G., Ke, J., Meng, X., Lu, S., Wu, X., Xu, H., Wu, F., Xu, Y., Xu, F., Bi, G.Q., Peng, G., Zhou, K., Zhu, Y., 2023. Distinct reward processing by subregions of the nucleus accumbens. Cell Rep. 42, 112069. https://doi.org/10.1016/j.celrep.2023.112069.

Chen, L., Lu, Y.P., Chen, H.Y., Huang, S.N., Guo, Y.R., Zhang, J.Y., Li, Q.X., Luo, C.Y., Lin, S.W., Chen, Z.N., Hu, L.H., Wang, W.X., Li, H.Y., Cai, P., Yu, C.X., 2020. Ventral tegmental area GABAergic neurons induce anxiety-like behaviors and promote palatable food intake. Neuropharmacology 173, 108114. https://doi.org/10.1016/j.neuropharm.2020.108114.

Chen, S., Xu, H., Dong, S., Xiao, L., 2022. Morpho-electric properties and diversity of oxytocin neurons in paraventricular nucleus of hypothalamus in female and male mice. J. Neurosci. 42, 2885–2904.

Chen, Z., Chen, G., Zhong, J., Jiang, S., Lai, S., Xu, H., Deng, X., Li, F., Lu, S., Zhou, K., Li, C., Liu, Z., Zhang, X., Zhu, Y., 2022. A circuit from lateral septum neurotensin neurons to tuberal nucleus controls hedonic feeding. Mol. Psychiatry 27, 4843–4860. https://doi.org/10.1038/s41380-022-01742-0.

Christoffel, D.J., Walsh, J.J., Heifets, B.D., Hoerbelt, P., Neuner, S., Sun, G., Ravikumar, V.K., Wu, H., Halpern, C.H., Malenka, R.C., 2021. Input-specific modulation of murine nucleus accumbens differentially regulates hedonic feeding. Nat. Commun. 12, 2135. https://doi.org/10.1038/s41467-021-22430-7.

Danjo, T., Yoshimi, K., Funabiki, K., Yawata, S., Nakanishi, S., 2014. Aversive behavior induced by optogenetic inactivation of ventral tegmental area dopamine neurons is mediated by dopamine D2 receptors in the nucleus accumbens. Proc. Natl. Acad. Sci. U. S. A 111, 6455–6460. https://doi.org/10.1073/pnas.1404323111.

Edwards, N.J., Tejeda, H.A., Pignatelli, M., Zhang, S., McDevitt, R.A., Wu, J., Bass, C.E., Bettler, B., Morales, M., Bonci, A., 2017. Circuit specificity in the inhibitory architecture of the VTA regulates cocaine-induced behavior. Nat. Neurosci. 20, 438–448. https://doi.org/10.1038/nn.4482.

Engelhard, B., Finkelstein, J., Cox, J., Fleming, W., Jang, H.J., Ornelas, S., Koay, S.A.,

Thiberge, S., Daw, N., Tank, D.W., Witten, I.B., 2019. Specialized and spatially organized coding of sensory, motor, and cognitive variables in midbrain dopamine neurons. Nature 570, 509–513. https://doi.org/10.1101/456194.

GBD 2017 Risk Factor Collaborators, 2018. Global, regional, and national comparative risk assessment of 84 behavioural, environmental and occupational, and metabolic risks or clusters of risks for 195 countries and territories, 1990-2017: a systematic analysis for the Global Burden of Disease Stu. Lancet 392, 1923–1994. https://doi.org/10.1016/S0140-6736(18)32225-6.

Gendelis, S., Inbar, D., Kupchik, Y.M., 2021. The role of the nucleus accumbens and ventral pallidum in feeding and obesity. Prog. Neuro-Psychopharmacol. Biol. Psychiatry 111, 110394. https://doi.org/10.1016/j.pnpbp.2021.110394.

Gong, S., Doughty, M., Harbaugh, C.R., Cummins, A., Hatten, M.E., Heintz, N., Gerfen, C.R., 2007. Targeting Cre recombinase to specific neuron populations with bacterial artificial chromosome constructs. J. Neurosci. 27, 9817–9823. https://doi.org/10.1523/JNEUROSCI.2707-07.2007.

Hajifathalian, K., Kumar, S., Newberry, C., Shah, S., Fortune, B., Krisko, T., Ortiz-Pujols, S., Zhou, X.K., Dannenberg, A.J., Kumar, R., Sharaiha, R.Z., 2020. Obesity is associated with worse outcomes in COVID-19: analysis of early data from New York City. Obesity 28, 1606–1612. https://doi.org/10.1002/oby.22923.

Han, Y., Xia, G., He, Yanlin, He, Yang, Farias, M., Xu, Y., Wu, Q., 2021. A hindbrain dopaminergic neural circuit prevents weight gain by reinforcing food satiation. eabf8719. Sci. Adv. 7. https://doi.org/10.1126/sciadv.abf8719.

He, Yanlin, Cai, X., Liu, Hailan, Conde, K.M., Xu, P., Li, Y., Wang, C., Yu, M., He, Yang, Liu, Hesong, Liang, C., Yang, T., Yang, Y., Yu, K., Wang, J., Zheng, R., Liu, F., Sun, Z., Heisler, L., Wu, Q., Tong, Q., Zhu, C., Shu, G., Xu, Y., 2021. 5-HT recruits distinct neurocircuits to inhibit hunger-driven and non-hunger-driven feeding. Mol. Psychiatry 26, 7211–7224. https://doi.org/10.1038/s41380-021-01220-z.

Heymsfield, S.B., Wadden, T.A., 2017. Mechanisms, pathophysiology, and management of obesity. N. Engl. J Med 376, 254–266. https://doi.org/10.1056/nejmra1514009.

Hommel, J.D., Trinko, R., Sears, R.M., Georgescu, D., Liu, Z.W., Gao, X.B., Thurmon, J.J., Marinelli, M., DiLeone, R.J., 2006. Leptin receptor signaling in midbrain dopamine neurons regulates feeding. Neuron 51, 801–810. https://doi.org/10.1016/j.neuron.2006.08.023.

Ilango, A., Kesner, A.J., Keller, K.L., Stuber, G.D., Bonci, A., Ikemoto, S., 2014. Similar roles of substantia nigra and ventral tegmental dopamine neurons in reward and aversion. J. Neurosci. 34, 817–822. https://doi.org/10.1523/JNEUROSCI.1703-13.2014.

Imoto, D., Yamamoto, I., Matsunaga, H., Yonekura, T., Lee, M.L., Kato, K.X., Yamasaki, T., Xu, S., Ishimoto, T., Yamagata, S., Otsuguro, K. ichi, Horiuchi, M., Iijima, N., Kimura, K., Toda, C., 2021. Refeeding activates neurons in the dorsomedial hypothalamus to inhibit food intake and promote positive valence. Mol. Metab. 54, 101366. https://doi.org/10.1016/j.molmet.2021.101366.

de Jong, J.W., Afjei, S.A., Pollak Dorocic, I., Peck, J.R., Liu, C., Kim, C.K., Tian, L., Deisseroth, K., Lammel, S., 2019. A neural circuit mechanism for encoding aversive stimuli in the mesolimbic dopamine system. Neuron 101, 133–151.e7. https://doi.org/10.1016/j.neuron.2018.11.005.

Kenny, P.J., 2011. Reward mechanisms in obesity: new insights and future directions. Neuron 69, 664–679. https://doi.org/10.1016/j.neuron.2011.02.016.

Klawonn, A.M., Malenka, R.C., 2018. Nucleus accumbens modulation in reward and aversion. Cold Spring Harb. Symp. Quant. Biol. 83, 119–129. https://doi.org/10.1101/sqb.2018.83.037457.

Krashes, M.J., Roth, B.L., Lowell, B.B., Krashes, M.J., Koda, S., Ye, C., Rogan, S.C., Adams, A.C., Cusher, D.S., Maratos-flier, E., Roth, B.L., Lowell, B.B., 2011. Rapid, reversible activation of AgRP neurons drives feeding behavior in mice. J. Clin. Invest 121, 1424–1428. https://doi.org/10.1172/JCI46229.1424.

Lammel, S., Hetzel, A., Haeckel, O., Jones, I., Liss, B., Roeper, J., 2008. Unique properties of mesoprefrontal neurons within a dual mesocorticolimbic dopamine system. Neuron 57, 760–773. . https://doi.org/DOI 10.1016/j.neuron.2008.01.022.

Lammel, S., Lim, B.K., Ran, C., Huang, K.W., Betley, M.J., Tye, K.M., Deisseroth, K., Malenka, R.C., 2012. Input-specific control of reward and aversion in the ventral tegmental area. Nature 491, 212–217. https://doi.org/10.1038/nature11527.

Land, B.B., Narayanan, N.S., Liu, R.J., Gianessi, C.A., Brayton, C.E., Grimaldi, M., Sarhan, D., Guarnieri, M., Deisseroth, D.J., Aghajanian, K., Dileone, R.J, G.K., 2014. Medial prefrontal D1 dopamine neurons control food intake. Nat. Neurosci. 17, 248–253. https://doi.org/10.1038/nn.3625.

Liu, Z., Le, Q., Lv, Y., Chen, X., Cui, J., Zhou, Y., Cheng, D., Ma, C., Su, X., Xiao, L., Yang, R., Zhang, J., Ma, L., Liu, X., 2022. A distinct D1-MSN subpopulation down-regulates dopamine to promote negative emotional state. Cell Res 32, 139–156. https://doi.org/10.1038/s41422-021-00588-5.

Low, A.Y.T., Goldstein, N., Gaunt, J.R., Huang, K.P., Zainolabidin, N., Yip, A.K.K., Carty, J.R.E., Choi, J.Y., Miller, A.M., Ho, H.S.T., Lenherr, C., Baltar, N., Azim, E., Sessions, O.M., Ch'ng, T.H., Bruce, A.S., Martin, L.E., Halko, M.A., Brady, R.O., Holsen, L.M., Alhadeff, A.L., Chen, A.I., Betley, J.N., 2021. Reverse-translational identification of a cerebellar satiation network. Nature 600, 269–273. https://doi.org/10.1038/s41586-021-04143-5.

Mahadevia, D., Saha, R., Manganaro, A., Morgan, A.A., Dumitriu, D., Rayport, S., Chuhma, N., Ziolkowski-blake, A., Ansorge, M.S., 2021. Dopamine promotes aggression in mice via ventral tegmental area to lateral septum projections. Nat. Commun. 12, 6796. https://doi.org/10.1038/s41467-021-27092-z.

Marino, R.A.M., McDevitt, R.A., Gantz, S.C., Shen, H., Pignatelli, M., Xin, W., Wise, R.A., Bonci, A., 2020. Control of food approach and eating by a GABAergic projection from lateral hypothalamus to dorsal pons. Proc. Natl. Acad. Sci. U. S. A 117, 8611–8615. https://doi.org/10.1073/pnas.1909340117.

Mazzone, C.M., Liang-Guallpa, J., Li, C., Wolcott, N.S., Boone, M.H., Southern, M., Kobzar, N.P., Salgado, I.D.A., Reddy, D.M., Sun, F., Zhang, Y., Li, Y., Cui, G., Krashes, M.J., 2020. High-fat food biases hypothalamic and mesolimbic expression of consummatory drives. Nat. Neurosci. 23, 1253–1266. https://doi.org/10.1038/s41593-020-0684-9.

Mebel, D.M., Wong, J.C.Y., Dong, Y.J., Borgland, S.L., 2012. Insulin in the ventral tegmental area reduces hedonic feeding and suppresses dopamine concentration via increased reuptake. Eur. J. Neurosci. 36, 2336–2346. https://doi.org/10.1111/j.1460-9568.2012.08168.x.

Morales, M., Margolis, E.B., 2017. Ventral tegmental area: cellular heterogeneity, connectivity and behaviour. Nat. Rev. Neurosci. 18, 73–85. https://doi.org/10.1038/nrn.2016.165.

Morton, G.J., Cummings, D.E., Baskin, D.G., Barsh, G.S., Schwartz, M.W., 2006. Central nervous system control of food intake and body weight. Nature. https://doi.org/10.1038/nature05026.

O'Connor, E.C., Kremer, Y., Lefort, S., Harada, M., Pascoli, V., Rohner, C., Lüscher, C., 2015. Accumbal D1R neurons projecting to lateral hypothalamus authorize feeding. Neuron 88, 553–564. https://doi.org/10.1016/j.neuron.2015.09.038.

Popkin, B.M., Du, S., Green, W.D., Beck, M.A., Algaith, T., Herbst, C.H., Alsukait, R.F., Alluhidan, M., Alazemi, N., Shekar, M., 2020. Individuals with obesity and COVID-19: A global perspective on the epidemiology and biological relationships. Obes. Rev. 21, e13128. https://doi.org/10.1111/obr.13128.

Poulin, J., Caronia, G., Hofer, C., Cui, Q., Helm, B., Awatramani, R., 2018. Mapping projections of molecularly defined dopamine neuron subtypes using intersectional genetic approaches. Nat. Neurosci. 21, 1260–1271. https://doi.org/10.1038/s41593-018-0203-4.

Roh, E., Song, D.K., Kim, M.S., 2016. Emerging role of the brain in the homeostatic regulation of energy and glucose metabolism. Exp. Mol. Med. 48, e216. https://doi.org/10.1038/emm.2016.4.

Rossi, M.A., Stuber, G.D., 2018. Overlapping brain circuits for homeostatic and hedonic feeding. Cell Metab. 27, 42–56. https://doi.org/10.1016/j.cmet.2017.09.021.

Saunders, A., Macosko, E.Z., Wysoker, A., Goldman, M., Krienen, F.M., de Rivera, H., Bien, E., Baum, M., Bortolin, L., Wang, S., Goeva, A., Nemesh, J., Kamitaki, N., Brumbaugh, S., Kulp, D., McCarroll, S.A., 2018. Molecular diversity and specializations among the cells of the adult mouse brain. Cell 174, 1015–1030.e16. https://doi.org/10.1016/j.cell.2018.07.028.

Shivacharan, R.S., Rolle, C.E., Barbosa, D.A.N., Cunningham, T.N., Feng, A., Johnson, N.D., Safer, D.L., Bohon, C., Keller, C., Buch, V.P., Parker, J.J., Azagury, D.E., Tass, P.A., Bhati, M.T., Malenka, R.C., Lock, J.D., Halpern, C.H., 2022. Pilot study of responsive nucleus accumbens deep brain stimulation for loss-of-control eating. Nat. Med. 28, 1791–1796. https://doi.org/10.1038/s41591-022-01941-w.

Sternson, S.M., 2016. Hunger: The carrot and the stick. Mol. Metab. 5, 1–2. https://doi.org/10.1016/j.molmet.2015.10.002.

Stuber, G.D., Wise, R.A., 2016. Lateral hypothalamic circuits for feeding and reward. Nat. Neurosci. 19, 198–205. https://doi.org/10.1038/nn.4220.

Swinburn, B.A., Sacks, G., Hall, K.D., McPherson, K., Finegood, D.T., Moodie, M.L., Gortmaker, S.L., 2011. The global obesity pandemic: shaped by global drivers and local environments. Lancet 378, 804–814. https://doi.org/10.1016/S0140-6736(11)60813-1.

Szczypka, M.S., Rainey, M.A., Kim, D.S., Alaynick, W.A., Marck, B.T., Matsumoto, A.M., Palmiter, R.D., 1999. Feeding behavior in dopamine-deficient mice. Proc. Natl. Acad. Sci. U. S. A 96, 12138–12143. https://doi.org/10.1073/pnas.96.21.12138.

Szczypka, M.S., Kwok, K., Brot, M.D., Marck, B.T., Matsumoto, A.M., Donahue, B.A., Palmiter, R.D., 2001. Dopamine production in the caudate putamen restores feeding in dopamine-deficient mice. Neuron 30, 819–828. https://doi.org/10.1016/S0896-6273(01)00319-1.

Tan, K.R., Yvon, C., Turiault, M., Mirzabekov, J.J., Doehner, J., Labouèbe, G., Deisseroth, K., Tye, K.M., Lüscher, C., 2012. GABA Neurons of the VTA Drive Conditioned Place Aversion. Neuron 73, 1173–1183. https://doi.org/10.1016/j.neuron.2012.02.015.

Tong, Q., Cui, X., Xu, H., Zhang, X., Hu, S., Huang, F., Xiao, L., 2023. D1 receptor-expressing neurons in ventral tegmental area alleviate mouse anxiety-like behaviors via glutamatergic projection to lateral septum. Mol. Psychiatry 28, 625–638. https://doi.org/10.1038/s41380-022-01809-y.

Van Zessen, R., Phillips, J.L., Budygin, E.A., Stuber, G.D., 2012. Activation of VTA GABA neurons disrupts reward consumption. Neuron 73, 1184–1194. https://doi.org/10.1016/j.neuron.2012.02.016.

Wang, X.F., Liu, J.J., Xia, J., Liu, J., Mirabella, V., Pang, Z.P., 2015. Endogenous glucagon-like peptide-1 suppresses high-fat food intake by reducing synaptic drive onto mesolimbic dopamine neurons. Cell Rep. 12, 726–733. https://doi.org/10.1016/j.celrep.2015.06.062.

Wise, R.A., Robble, M.A., 2020. Dopamine and addiction. Annu. Rev. Psychol. 71, 79–106. https://doi.org/10.1146/annurev-psych-010418-103337.

Xiao, L., Priest, M.F., Kozorovitskiy, Y., 2018. Oxytocin functions as a spatiotemporal filter for excitatory synaptic inputs to VTA dopamine neurons. Elife 7, e33892. https://doi.org/10.7554/eLife.33892.

Yang, H., de Jong, J.W., Tak, Y.E., Peck, J., Bateup, H.S., Lammel, S., 2018. Nucleus accumbens subnuclei regulate motivated behavior via direct inhibition and disinhibition of VTA dopamine subpopulations. Neuron 97, 434–449.e4. https://doi.org/10.1016/j.neuron.2017.12.022.

Zhou, Q.Y., Palmiter, R.D., 1995. Dopamine-deficient mice are severely hypoactive, adipsic, and aphagic. Cell 83, 1197–1209. https://doi.org/10.1016/0092-8674(95)90145-0.

Zingg, B., Peng, B., Huang, J., Tao, H.W., Zhang, L.I., 2020. Synaptic specificity and application of anterograde transsynaptic AAV for probing neural circuitry. J. Neurosci. 40, 3250–3267. https://doi.org/10.1523/JNEUROSCI.2158-19.2020.